Journal of Experimental & Clinical Cancer Research

RESEARCH

Open Access

Cancer-educated mammary adipose tissue-derived stromal/stem cells in obesity and breast cancer: spatial regulation and function

Andreas Ritter*, Nina-Naomi Kreis, Susanne Roth, Alexandra Friemel, Babek Kahn Safdar, Samira Catharina Hoock, Julia Maria Wildner, Roman Allert, Frank Louwen, Christine Solbach† and Juping Yuan*†

Abstract

Background Breast cancer is the most frequently diagnosed cancer and a common cause of cancer-related death in women. It is well recognized that obesity is associated with an enhanced risk of more aggressive breast cancer as well as reduced patient survival. Breast adipose tissue-derived mesenchymal stromal/stem cells (bASCs) are crucial components of the tumor microenvironment. A key step initially involved in this process might be the de-differentiation of bASCs into tumor supporting phenotypes.

Methods In the present work, we isolated bASCs from adipose tissues adjacent to the tumor (aT bASCs) from lean- (ln-aT bASCs, BMI ≤ 25) and breast cancer patients with obesity (ob-aT bASCs, BMI ≥ 35), and analyzed their phenotypes with functional assays and RNA sequencing, compared to their counterparts isolated from adipose tissues distant from the tumor (dT bASCs).

Results We show that ln-aT bASCs are susceptible to be transformed into an inflammatory cancer-associated phenotype, whereas ob-aT bASCs are prone to be cancer-educated into a myofibroblastic phenotype. Both ln-aT- and ob-aT bASCs compromise their physiological differentiation capacity, and upregulate metastasis-promoting factors. While ln-aT bASCs stimulate proliferation, motility and chemoresistance by inducing epithelial-mesenchymal transition of low malignant breast cancer cells, ob-aT bASCs trigger more efficiently a cancer stem cell phenotype in highly malignant breast cancer cells.

Conclusion Breast cancer-associated bASCs are able to foster malignancy of breast cancer cells by multiple mechanisms, especially, induction of epithelial-mesenchymal transition and activation of stemness-associated genes in breast cancer cells. Blocking the de-differentiation of bASCs in the tumor microenvironment could be a novel strategy to develop an effective intervention for breast cancer patients.

Significance This study provides mechanistic insights into how obesity affects the phenotype of bASCs in the TME. Moreover, it highlights the molecular changes inside breast cancer cells upon cell-cell interaction with cancer-educated bASCs.

Keywords Breast adipose tissue-derived mesenchymal stromal/stem cells, Cancer-associated fibroblasts, Obesity, Breast cancer, Epithelial-to-mesenchymal transition, Chemoresistance, Cancer stem cells, Tumor microenvironment

†Christine Solbach and Juping Yuan contributed equally to this work.

*Correspondence:
Andreas Ritter
Andreas.Ritter@kgu.de
Juping Yuan
yuan@em.uni-frankfurt.de
Full list of author information is available at the end of the article

Graphical abstract

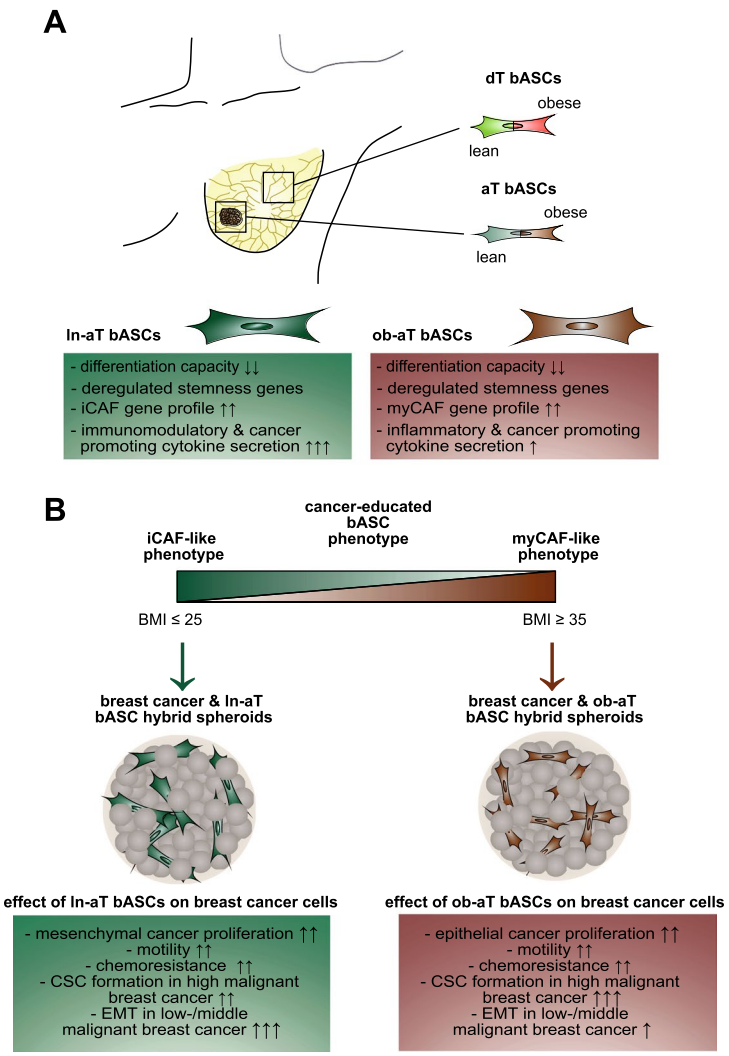

Background

The prevalence of obesity has been increasing in recent decades and has more than doubled worldwide since 1980 [1], posing a big challenge to the entire society and health care systems [2, 3]. Obesity is associated with enhanced risk of more aggressive breast cancer as well as reduced survival of postmenopausal breast cancer patients [4]. Despite intensive research, the relationship between obesity and breast cancer development is still not completely understood. Adipocyte hypertrophy during the development of obesity induces hypoxic conditions within the adipose tissue and results in chronic and systemic inflammation, endoplasmic reticulum (ER) stress, and altered extracellular matrix (ECM) composition [5]. In addition, obesity, indicated by body mass index (BMI) over 30, interferes with the immune system including the activation of macrophages via toll-like receptors 4 (TLR4), which stimulates nuclear factor kappa B (NFκB) signaling und further fuels inflammation of adipose tissue [6]. These changes lead adipocytes and stromal cells to produce pro-inflammatory cytokines, including interleukin 6 (IL6), IL1β and tumor necrosis factor α (TNF-α), and growth factors, such as insulin, insulin-like growth factor 1 (IGF-1) and leptin [7, 8]. Increased cytokines and chemokines are further accompanied by increased infiltration of immune cells, cellular stress, hypoxia, insulin resistance, glucose intolerance, adipocyte hypertrophy and hyperplasia, and impaired tissue homeostasis [9]. Most of these enumerated alterations

including increased growth factors, hypoxia and deregulated immune response are well known to promote breast cancer development and progression [10]. Although high serum levels of insulin, leptin and estradiol have been proposed to activate diverse signaling cascades and contribute to the progression of postmenopausal breast cancer of patients with obesity [4, 11], however, the molecular mechanisms by which obesity correlates with premenopausal breast cancer remain to be unraveled.

The tumor microenvironment (TME) is crucial for breast cancer progression, which has been the subject of intense research and is influenced by high grade of obesity [12]. Breast cancer is mainly surrounded by mammary adipose tissue, which contains a multitude of cell types, such as endothelial cells, progenitor cells, immune cells, fibroblasts and mesenchymal stromal/stem cells (MSCs), which, together with soluble factors as well as insoluble ECM proteins secreted by adipocytes, stromal cells and cancer cells, constitute the TME [13–15]. Among these cell types, fibroblasts have attracted high attention, as they are capable of de-differentiation into several types of cancer-associated fibroblasts (CAFs) in the TME of breast cancer, including a myofibroblastic (myCAF) and an inflammatory (iCAF) subgroup [16]. These CAFs promote tumor growth, invasion, metastasis and resistance to chemotherapeutics of breast cancer cells by secreting factors including CC-chemokine-ligand 2 (CCL2), C-X-C motif ligand 1–3 (CXCL1–3), and IL6, stiffening the ECM, affecting cancer cell metabolism [17], interacting with and influencing the functions of diverse stromal cells, such as MSCs, endothelial, and immune cells [16].

MSCs are a multipotent cell type and exist in diverse organs and tissues. They are involved in the maintenance of tissue homeostasis, regulation of local immune response, and repair of damaged tissues [18]. Beside their high differentiation capacity, they share many features with fibroblasts such as similar surface markers, morphology, gene expression profiles and proliferation rates [19]. As a result, much attention has also been paid to how different MSC subtypes contribute to breast cancer progression. However, most of these studies were based on MSCs isolated from non-breast sources, such as abdominal adipose tissue, bone marrow and peripheral blood [20–22]. MSCs from different tissues have distinct transcriptomic, biochemical, and secretory profiles as well as biological functions [23, 24]. This leads to bivalent results with tumor-supportive and -suppressive functions [25, 26], which may not reflect the in vivo situation in breast cancer tissue.

Little is known about the involvement of adipose tissue-derived mesenchymal stromal/stem cells (bASCs) isolated directly from mammary adipose tissues surrounding breast cancer. To investigate the bidirectional relationship between breast cancer cells and bASCs, we isolated bASCs from mammary adipose tissue adjacent ($\leq$ 3 cm, −aT) to the tumors of lean (ln, BMI $\leq$ 25) or breast cancer patients with obesity (ob, BMI $\geq$ 35) and analyzed their phenotypes, compared to their control counterparts isolated from mammary adipose tissue distant to the tumors ($\geq$ 9 cm, −dT) from the same patients. We show that these breast cancer associated bASCs highly reduce their differentiation capacity and alter their cytokine and chemokine secretion pattern. Interestingly, like fibroblasts, bASCs are also able to de-differentiate into at least two types of CAF-like cells that stimulate proliferation, motility and chemoresistance of low- as well as high-malignant breast cancer cells in 3D-spheroids, supporting the tumorigenic behavior of bASCs in the TME.

Methods

bASC isolation, cell lines, cell culture and differentiation

This study is approved by the Ethics Committee of the Johann Wolfgang Goethe-University Hospital Frankfurt (reference number: 443/11 and 4/09) and informed written consent was obtained from all donors. Mammary adipose tissue was obtained at least 9 cm distant from the tumor site (dT) and maximal 3 cm adjacent to the tumor site (aT) from the same women undergoing breast cancer surgery. Clinical information of patients is detailed in Table S1. bASCs were isolated as described [20] with modifications. In brief, obtained dT and aT adipose tissues were immediately washed, minced to small pieces, and digested with 1 mg/ml collagenase type I for 1 h, 200 rpm at 37 °C. Cells were pelleted by centrifugation at 700 g for 10 min and filtered through a 100 µm mesh filter to remove undigested adipose tissue. The remaining blood cells were lysed by addition of red blood cell lysis buffer (155 mM NH_4Cl, 10 mM $KHCO_3$, and 0.1 mM EDTA) for 10 min at 37 °C. To remove the lysis buffer, cells were centrifuged at 700 g for 10 min. The remaining cells were centrifuged, seeded onto 6-cm cell culture plates in DMEM containing 20% fetal bovine serum (FBS), 100 mg/ml streptomycin, 100 U/ml penicillin, 2 mM l-glutamine, and 1 g/ml amphotericin-B and cultured under standard cell culture conditions. After 24 h, non-adherent cells were removed and the remaining cells were washed, cultured, expanded and characterized (ln: Table S2, ob: Table S3). Early passages (P2 to P6) of isolated bASCs were used for experiments. The cells isolated from patients treated with tamoxifen (TMX) or radiotherapy were excluded for transcriptomic analysis. Breast cancer cell lines were chosen based on their cell surface receptor composition, namely estrogen (ER),

progesterone (PR) and human epidermal growth factor receptor 2 (HER2) [27], and their malignancy potential (low/intermediate/high). The breast cancer cell lines BT474$^{(ER+,\ PR+,\ HER2+,\ low)}$, MDA-MB-361$^{(ER+,\ PR+/-,\ HER2+,\ intermediate)}$, MCF-7$^{(ER+,\ PR+,\ HER2+,\ low)}$ and MDA-MB-231$^{(ER-,\ PR-,\ HER2-)}$) were obtained from ATCC (Wesel, Germany). All cells were cultured as instructed.

The differentiation of bASCs toward adipogenic, osteogenic and chondrogenic lineages are detailed in supplementary information.

Cell viability, cell cycle distribution and flow cytometry (FACS)

Cell viability, cell cycle distribution and FACS of bASCs and breast cancer cell lines are detailed in supplementary information.

Indirect immunofluorescence staining, immunohistochemistry of breast cancer tissue, imaging and signal intensity measurement

The indirect immunofluorescence staining, immunohistochemistry staining of breast cancer tissue, image acquisition, primary and secondary antibodies and signal intensity quantification are detailed in supplementary information.

Western blot analysis

Western blot analysis, primary and secondary antibodies are detailed in supplementary information.

RNA extraction, real-time PCR (qPCR) and transcriptomic analysis (RNA-seq)

RNA extraction, qPCR, probes and RNA-seq are detailed in supplementary information.

Human cytokine array and ELISA

Human cytokine array and ELISA quantifications are detailed in supplementary information.

Spheroid formation, mitotic index,spheroid proliferation and epithelial-to-mesenchymal transition (EMT) analysis

The spheroid formation, mitotic index, EMT and spheroid proliferation assays are described in supplementary information and as reported [28].

Motility assay

The motility assay is described in supplementary information and the patterns of motility were evaluated as reported [29].

Spheroid cell viability, foci analysis and live/dead cell assay

Spheroid cell viability, foci analysis and live/dead cell assay are detailed in supplementary information.

Statistical analysis

Before statistical analysis, an outlier test was performed with all data sets. Student's t-test (two tailed and paired or homoscedastic) was used to evaluate the significance of difference between diverse groups for gene analysis, cell viability assay, cell cycle distribution and western blot analysis. The statistical evaluation of the single cell tracking assay, immunofluorescence quantification, spheroid evaluation, foci quantification, live/dead fluorescence quantification was performed by using an unpaired Mann-Whitney U test (two tailed). Difference is considered as statistically significant when $p < 0.05$.

Results

Lean and obese bASCs reduce their differentiation capacity within the TME

The importance of the differentiation capacity of MSCs is well-known for proper tissue homeostasis and regeneration [30, 31]. We questioned how the TME would affect the differentiation capacity of ln-aT bASCs and ob-aT bASCs, compared to their counterpart ln-dT bASCs and ob-dT bASCs isolated from adipose tissue distant to the tumors. Clinical information of the patients is listed in Table S1. These bASCs were subjected to adipogenic, osteogenic and chondrogenic differentiation stimuli and their differentiation capacities were evaluated by lineage specific staining and gene analysis. The analysis showed that ob-bASCs had a highly reduced differentiation capacity in all three analyzed lineages compared to ln-bASCs (Fig. 1), supporting our previous reports of visceral and subcutaneous ASCs [9, 32, 33]. Specifically, both ln- and ob-aT bASCs displayed a significantly reduced adipogenic differentiation capacity compared to ln- and ob-dT bASCs (Fig. 1A-D). In accordance, ln-dT bASCs had the highest percentage of immature- (44.2%) and mature adipocytes (24.1%), compared to the other three subgroups (Fig. 1A-C). Although ob-dT bASCs showed no difference in the percentage of immature adipocytes relative to ob-aT bASCs (ob-dT bASCs: 28.5% vs. ob-aT bASCs: 27.7%) (Fig. 1A and B, 4th and 5th bars), the ob-dT bASCs displayed a significantly increased number of mature adipocytes (ob-dT bASCs: 17.0% vs. ob-aT bASCs: 8.6%) (Fig. 1A and C, 4th and 5th bars), suggesting a reduction of adipogenic differentiation ability of ob-aT bASCs. In line with this observation, the expression of adipogenic-related genes such as peroxisome proliferator-activated receptor γ (*PPARγ)*, adiponectin (ADIPOQ) and *LEPTIN* were highly upregulated by 66–83% in ln-dT bASCs compared to ln-aT bASCs (Fig. 1D, 5th vs. 6th bar). Reduced adipogenic gene expression was also observed in ob-aT bASCs in comparison to ob-dT bASCs (Fig. 1D, 7th vs. 8th bar), yet not to the same extent as in ln bASCs, and a significant difference was observed only for *PPARγ*.

Similar results were obtained from microscopic analyses of the calcium deposition in differentiated osteocytes stained with Alizarin Red S (Fig. 1E). Compared to dT bASCs, aT bASCs demonstrated a reduced percentage of differentiated osteocytes and a lower mean gray value, a parameter used for the evaluation of the staining signal [34], of the Alizarin Red S staining (Fig. 1E-G, 2nd vs. 3rd bar and 4th vs. 5th bar). In particular, ob-dT bASCs had a decreased differentiation capacity by 11% (Fig. 1E-G, 3nd vs. 5th bar). Consistent with these results, all five genes *KLF4*, *PTCH1*, *c-MYC*, *OSTEOPONTIN* and *RUNX2* associated with osteogenic differentiation were significantly higher in ln- and ob-dT bASCs compared to ln- and ob-aT bASCs (Fig. 1H). In further support, the chondrogenic differentiation, indicated with the specific staining of Alcian blue used to identify sulfated proteoglycans, showed a comparable trend (Fig. 1I and J). bASCs in the proximity of breast cancers exhibited drastically reduced chondrogenic differentiation capacity, as indicated by a weaker staining of polysaccharides quantified by the mean gray value (Fig. 1I, 2nd and 4th bars). Both distant bASCs subgroups displayed a moderate blue staining, whereas ln-dT bASCs showed a 26% increased gray value compared to ob-dT bASCs (Fig. 1I, 3rd vs. 5th bars). These results clearly demonstrate an impaired differentiation capability of obese- and cancer-near bASCs, suggesting a cancer-educated phenotype of bASCs in the TME of breast cancers.

To exclude the possibility that these differentiation alterations were a result of a changed cell cycle distribution or cell proliferation, cell cycle analyses and cell viability assays were performed. None of the analyzed bASC groups (ln/ob-aT/dT) showed significant differences in both assays (Fig. S1A and B). Moreover, all bASCs subgroups displayed a comparable CD (cluster of differentiation) marker profile specific for MSCs (Table S2 and S3) [35].

bASCs de-differentiate into distinct CAF-like phenotypes

Tumors are known to shape their TME to support their development, proliferation, metastasis and therapeutic resistance [36]. Especially, CAFs derived from various cell origins such as fibroblasts and MSCs [16, 37] are key components of the TME and important in TME remodeling [38]. To address if aT-bASCs de-differentiate into a myofibroblastic cancer-associated (myCAF) phenotype, we assessed their specific protein markers alpha-smooth muscle actin (αSMA), fibroblast-specific protein1 (FSP1) and integrin subunit beta 1 (CD29) by flow cytometry. As presented in Fig. 2A-C, ln-aT bASCs showed a moderately increased expression of αSMA and CD29 compared to ln-dT bASCs (Fig. 2A and C, 1st vs. 2nd bar). FSP1 did not show any differences in these lean bASCs subtypes (Fig. 2B, 1st vs. 2nd bar). Interestingly, ob-aT bASCs displayed a significantly enhanced expression of all three myCAF marker proteins in comparison to ob-dT bASCs (Fig. 2A-C, 3rd vs. 4th bar). CAFs, isolated from the same breast cancer as reported [39] and served as positive control, showed a remarkably high expression of αSMA and FSP1 (Fig. 2A and B, 5th and 6th bar), whereas CD29 was only upregulated in CAFs isolated from patients with obesity, similar to ob-aT bASCs (Fig. 2C, 3th and 6th bars).

To corroborate these results, bASCs were stained for αSMA, vimentin (VIM) and collagen type I alpha 1 chain (COL1A1) for intensity quantification. The analyses revealed elevated signals for αSMA, VIM and COL1A1 in ln/ob-aT bASCs (Fig. 2D and E, Fig. S1C-F), whereas ln/ob-dT bASCs only displayed low to moderate staining signals (Fig. 2D and E, Fig. S1C-F). Of note, the expression of COL1A1 in bASCs could be clustered into three groups (Fig. S1C, E and F): the majority of lean and obese dT bASCs had a low expression of COL1A1 (Fig. S1C and F, 1st and 3rd bars), a high expression was observed in ln/ob-aT bASCs (Fig. S1C and F), and a high percentage of ob-aT bASCs also presented intermediate levels (Fig. S1C and F).

(See figure on next page.)

Fig. 1 Lean and obese bASCs adjacent to breast cancer display an impaired differentiation capacity. **A-J** bASCs (ln-aT, ln-dT, ob-aT and ob-dT) were induced to adipogenic (adipo. Diff.) (**A**-**D**) for 14 days, osteogenic (osteo. Diff.) (**E**-**H**) and chondrogenic differentiation (chondro. Diff.) (**I** and **J**) for 21 days and their differentiation rates were evaluated. ln-dT bASCs were used as control cells without differentiation medium. **A** bASCs were stained for α-tubulin (green), phalloidin (red) to visualize the cytoskeleton, and DNA (DAPI, blue). Example images are shown. Scale bar: 50 µm. **B** and **C** The percentage of immature adipocytes (lipid vacuoles < 5 nm) (**B**) or mature adipocytes (lipid vacuoles > 5 nm) (**C**) was quantified. The results of individual bASC subgroups are presented as mean ± SEM ($n = 500$ cells for each condition, pooled from three experiments). **D** The gene expression of *PPARγ*, *ADIPOQ* and *LEPTIN* is shown for undifferentiated (−) and differentiated (+) bASCs. The results are from three individual experiments and presented as mean ± SEM. **E** bASCs were stained with Alizarin Red S to visualize calcium deposition. Representative images are shown. Scale bar: 50 µm. **F** and **G** The percentage of bASCs showing calcium deposition (**F**) and the mean gray value (**G**) were evaluated. The results are presented as mean ± SEM (F: n = 500 cells for each condition, pooled from three experiments, G: $n = 30$ images for each condition, pooled from three experiments). **H** The gene expression of *KLF4*, *PTCH1*, *c-MYC*, *OSTEOPONTIN* and *RUNX2* is shown for undifferentiated (−) and differentiated (+) bASCs. The results are from three individual experiments and presented as mean ± SEM. **I** and **J** bASCs were stained with Alcian blue to visualize acidic polysaccharides. Representative bright-field images are shown (**J**). Scale bar: 50 µm. The quantification of the mean gray value is presented (**I**). The results are shown as mean ± SEM ($n = 30$ images for each condition, pooled from three experiments). Unpaired Mann-Whitney U test was used in (**B** and **C**), (**F** and **G**) and (**I**). $*p < 0.05$, $**p < 0.01$, $***p < 0.001$. Student's t test was used in (**D**) and (**H**). $*p < 0.05$, $**p < 0.01$, $***p < 0.001$

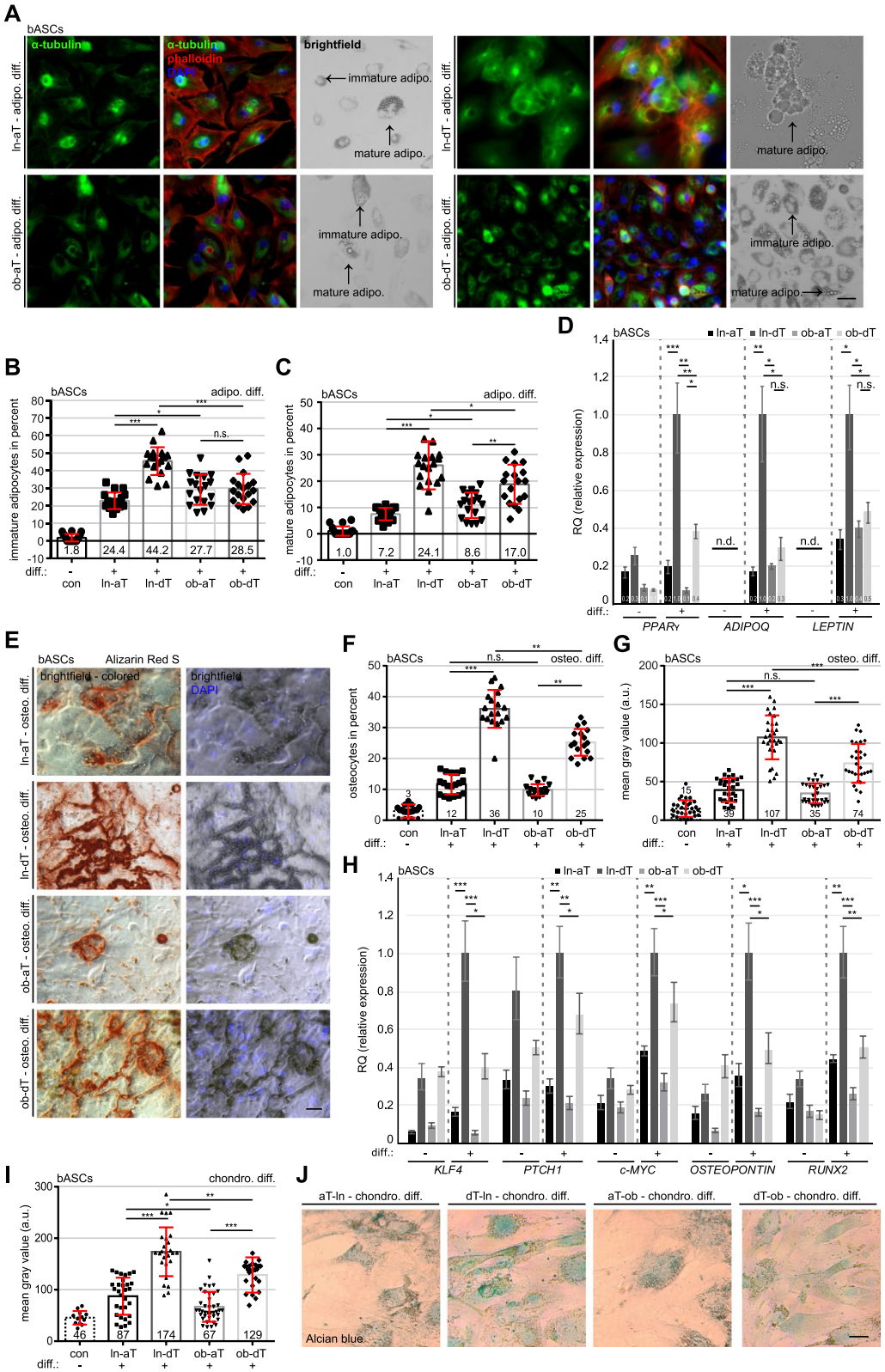

Fig. 1 (See legend on previous page.)

Furthermore, we analyzed the protein levels of αSMA, COL1A1, pAKT, AKT and pGSK3β via Western blot analysis. ob-aT bASCs presented an upregulated αSMA compared to all other bASC subgroups (Fig. 2F and G). By contrast, αSMA was just marginally increased in ln-aT bASCs (Fig. 2F and G), but COL1A1 was increased in ln-aT bASCs as indicated by the previous immunofluorescence staining (Fig. 2F and Fig. S1C, E and F). Moreover, ln-aT bASCs, like ob-aT bASCs, showed an activated PI3K pathway evidenced by increased pAKT and pGSK3β (Fig. 2F).

Unlike ob-aT bASCS, ln-aT bASCs displayed an inconclusive expression of specific myCAF markers. We hypothesized that ob-aT bASCs represented a myCAF-like type, whereas ln-aT bASCs might exhibit a different cancer-associated phenotype, namely iCAF, as described for fibroblasts [40, 41]. To clarify this issue, gene expression analysis of the myCAF associated genes *ACTA2*, connective tissue growth factor (*CTGF)* and transgelin (*TAGLN),* and iCAF classified genes colony stimulating factor 3 (*CSF3)*, *CXCL10*, *IL1β* and hyaluronan synthase 1 (*HAS1)* [40, 42] were performed. Indeed, these analyses revealed that ob-aT bASCs had a predominant myCAF phenotype with highly increased gene levels of *ACTA2*, *TAGLN* and *CTGF* compared to ln-dT bASCs (Fig. 2H, 2nd vs. 3rd bar). Strikingly, though displaying slightly elevated gene profiles of *ACTA2* and *CTGF* (Fig. 2H, 1st vs. 2nd bar), ln-aT bASCs had a significantly increased expression of iCAF genes including *CSF3*, *CXCL10* and *IL1β* (Fig. 2I, 1st vs. 2nd bar). The gene levels of *HAS1* were low and not significantly altered in bASCs, because of the low gene copy number (Fig. 2I, 4th graph). Ob-aT bASCs mostly had lower expression of these genes compared to other bASCs (Fig. 2I). These results suggest that bASCs in the TME are de-differentiated toward CAF-like phenotypes, which explains the greatly reduced differentiation capacity of both bASCs subgroups. Furthermore, these data highlight that obesity impacts the de-differentiation of bASCs isolated from adipose tissue near the breast tumor. Of importance, ln-aT bASCs reflected the gene expression pattern of an iCAF-like phenotype, whereas ob-aT bASCs demonstrated a myCAF gene and protein profile.

Transcriptional reprogramming of bASCs in the TME

Since ln/ob-aT bASCs displayed a functional decline and a transition to cancer-educated bASC phenotypes, a transcriptomic analysis should reveal the impact of the TME on the overall gene expression of aT bASCs in comparison to dT bASCs. Total RNAs were extracted from the four bASC subgroups for whole-genome mRNA-sequencing (RNA-seq) [43]. Strikingly, the transcriptome analysis revealed 967 deregulated genes with a significantly adjusted *p*-value in ln-aT bASCs versus ln-dT bASCs visualized by a heatmap (Fig. 3A) and a volcano plot (Fig. 3C). The transcriptome comparison between ob-aT bASCs and ob-dT bASCs revealed 824 significantly deregulated genes by using the *p*-value without adjustment (Fig. 3B and Fig. 3D), possibly due to distinct gene alterations in each obese individual. The "Kyoto Encyclopedia of Genes and Genomes" (KEGG) pathway analysis highlighted the most significant changes in their gene expression of ln-aT bASCs in the cell-cell receptor interaction (33 genes), pathways in cancer (40 genes), TNF signaling pathway (20 genes), PI3K-Akt signaling pathway (30 genes), and the chemokine signaling pathway (23 genes), compared to ln-dT bASCs (Fig. 3E). Interestingly, a further pathway analysis by the "Gene Ontology project" (GO) revealed that pathways involved in immune system processes (187 genes), response to stress (256 genes), signal transduction (337 genes) and cell differentiation (219 genes) were altered in ln-aT bASCs (Fig. 3F). The altered genes in the cell differentiation pathway included stemness- and proliferation-associated genes such as Erb-B2 receptor tyrosine kinase 4 (*ERBB4)*, roundabout guidance receptor 2 (*ROBO2)*, slit guidance ligand 2 (*SLIT2)*, forkhead box C2 (*FOXC2*), SRY-box transcription factor 9 (*SOX9)*, hyaluronan synthase 2 (*HAS2)*, retinoblastoma-associated protein 1 (*E2F1)*, forkhead box L1 (*FOXL1)* and nuclear factor

(See figure on next page.)

Fig. 2 The tumor microenvironment induces the de-differentiation of bASCs. **A-C** bASCs (ln-aT, ln-dT, ob-aT and ob-dT) were stained for αSMA, FSP1 and CD29 for FACS analyses. CAFs (ln-CAF and ob-CAF) were isolated and stained as positive controls. Quantification of αSMA (**A**), FPS1 (**B**) and CD29 (**C**) are shown as bar graphs. The results are from three independent experiments ($n = 3$, 60.000 cells for each condition and in each group) and presented as mean ± SEM. **D** Representative images of bASCs and CAFs stained for αSMA (green), phalloidin (red) and DNA (DAPI, blue) are shown. Red boxes indicate measured areas. Scale: 25 µm. Inset scale: 12.5 µm. **E** The evaluation of the mean fluorescence intensity of αSMA is presented as scatter plots. The results are from three independent experiments ($n = 3$, 90 cells for each condition and in each group) and presented as mean ± SEM. **F** Cellular extracts from bASCs were prepared for WB analysis with antibodies against αSMA, COL1A1, caveolin-1, AKT, pAKT and pGSK3β. GAPDH and β-actin served as loading controls. **G** Quantification of the αSMA signal in WB is shown, relative to the corresponding amount of GAPDH. The results are from three independent experiments and presented as mean ± SEM. **H** and **I** Relative gene levels of *ACTA2*, *TAGLN* and *CTGF,* important myCAF marker genes (**H**), and relative gene expression of *CSF3*, *CXCL10*, *IL1β* and HAS1, iCAF marker genes (**I**), are shown for bASC subgroups (ln-dT, ln-aT, ob-dT and ob-aT). The results are from three independent experiments and presented as bar graphs with mean ± SEM. Student's t test was used in (**A**-**C**) and (**G**-**I**). Unpaired Mann-Whitney U test was used in (**E**). $*p < 0.05$, $**p < 0.01$, $***p < 0.001$. $*p < 0.05$, $***p < 0.001$

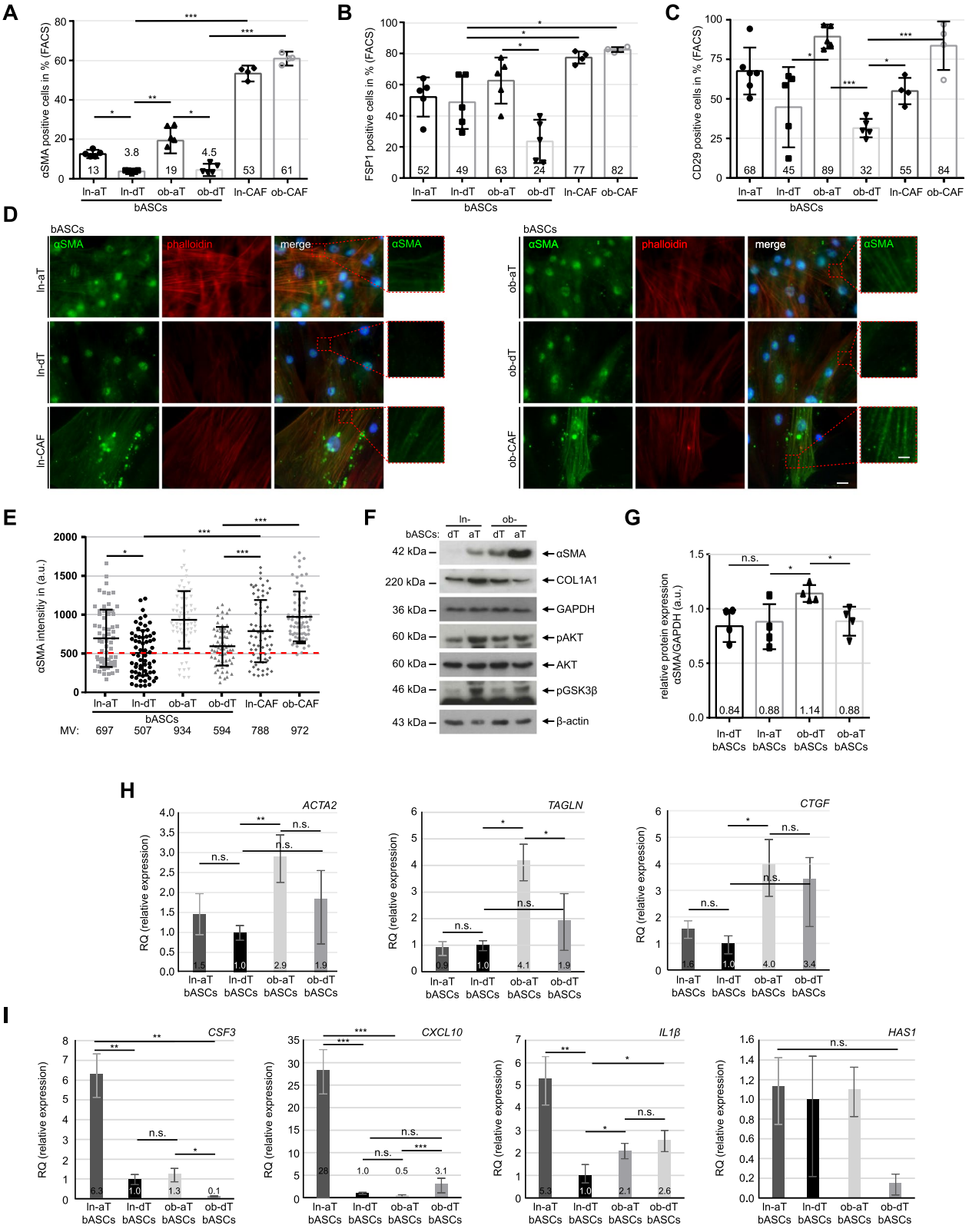

Fig. 2 (See legend on previous page.)

kappa b subunit 2 (*NFκB2)*, all of which were upregulated in ln-aT bASCs (Fig. S2A, 1st to 9th plots). Their downregulated genes included platelet derived growth factor receptor beta (*PDGFRβ)*, androgen receptor (*AR)* and homeobox A2 (*HOXA2)* (Fig. S2A, 10th to 12th plots).

Transcriptome analysis corroborated the gene expression of myCAFs (Fig. 3G, 1st to 3rd plots). Important myCAF genes, including *ACTA2*, *TAGLN* and *CTGF,* were upregulated in ob-aT bASCs (Fig. 3G, 1st to 3rd plots), whereas ln-aT bASCs showed an increased expression of iCAF associated genes such as *CCL2*, leukemia inhibitory factor (*LIF)*, *IL1β*, *CSF3* and *HAS1* (Fig. 3G, 4th to 8th plots). In addition, ln-aT bASCs displayed various upregulated cytokine genes including *IL8*, *CXCL1–3* and *CXCL10* reported for iCAFs (Fig. S2B). Moreover, presented with a heatmap, ln-aT bASCs displayed a prominent iCAF phenotype by showing an upregulated gene expression of chemokines, including *CCL*, colony stimulating factor (*CSF*), C-C motif chemokine receptor 5 (*CCR5*), *CXCL*, cytokines such as *IL1A*, *IL1B*, *IL18BP*, the IL1 receptor accessory protein (*IL1RAP*), *LIF*, and growth factors including vascular endothelial growth factor C (*VEGFC*), *PDGFB* and its receptor *PDGFRB* (Fig. 3H). In sum, the transcriptome analysis supports the notion that the TME greatly impacts the function and biology of bASCs. In particular, the TME educates ln-aT bASCs into an iCAF-like phenotype displaying a high gene expression of cytokines, chemokines and growth factors.

dT bASCs alter their cytokine secretion upon co-culture with triple negative breast cancer cells

Transcriptome analysis revealed a network of deregulated cytokines in bASCs isolated adjacent to breast cancer cells (Fig. 3H). To look at the secretion profiles of these cytokines, the conditioned media from bASCs were collected for evaluation using a human cytokine array containing 120 different targets. ln-aT as well as ob-aT bASCs secreted a higher amount of important migration and invasion stimulatory cytokines such as CXCL5, CXCL6, CXCL11, CCL27, IL8, the tissue inhibitor of metalloproteinase 1 (TIMP-1), the macrophage migration inhibiting factor (MIF), and the interleukin 6 signal transducer (IL6ST, also known as gp130 and IL6R-β) (Fig. S3A and B). CXCL11 was the only cytokine, which was significantly upregulated in ob-aT bASCs compared to ob-dT bASCs (Fig. S3B, 2ndgraph).

To investigate the impact of breast cancer cells on the cytokine secretion of bASCs, all subgroups of bASCs were indirectly co-cultured (Fig. S2C) with the triple negative breast cancer cell line MDA-MB-231 for 7 days. The cells were then cultured in serum-free medium for additional 3 days for collecting conditioned media for cytokine evaluation. Surprisingly, 7-day indirect co-culture with MDA-MB-231 cells was sufficient to induce an altered secretion pattern in dT bASC control cells (Fig. S3A, 2nd vs. 6th, and 4th vs. 8th row). By contrast, this indirect co-culture did not influence aT bASCs to the same extent as dT ASCs (Fig. S3A, 1st vs. 5th and 3rd vs. 7th row). Intriguingly, both ln/ob dT-bASCs significantly increased their secretion of stem cell factor (SCF), CCL5, VEGFA, oncostatin M (OSM), MIF, and osteoprotegerin (OPG) (Fig. S3C). In addition, the secretion of CXCL1 and CXCL5, two cytokines involved in breast cancer metastasis [44, 45], was moderately increased in all subgroups after indirect co-culture with MDA-MB-231 cells (Fig. S3D). These results highlight the importance of the interaction between breast cancer cells, the TME and bASCs, even an indirect short co-culture in this experimental setup, already partially educate dT bASCs by altering their secretion pattern of various cytokines.

Ln- and Ob-aT bASCs upregulate the gene expression and secretion of tumor promoting cytokines

To further corroborate the transcriptome analysis data, we extracted RNA from four bASCs subgroups for quantitative gene analysis. Compared to ln-dT bASCs, ln-aT bASCs showed increased gene expression of *IL6*, *IL8*, *CXCL1–3*, *CCL2*, *VEGFC*, fibroblast growth factor 1 (*FGF1*) and *FGF*2, and *LIF* (Fig. 4A, 1st vs. 2nd bar) supporting the finding from the transcriptome analysis (Fig. 3H and Fig. S2B). The most significant hits were *LIF*, *CXCL1, CXCL2* and *CXCL3*, which were all highly upregulated

(See figure on next page.)

Fig. 3 Transcriptomic profiles of lean and obese bASCs adjacent to breast cancers. **A**-**G** Total RNAs were extracted from each sample of bASC subgroups (ln-dT, ln-aT, ob-dT and ob-aT, 5 samples for each subgroup) for transcriptome analysis. **A** and **B** Heatmap of significantly differentially expressed genes of ln-dT vs. ln-aT bASCs (**A**) and ob-dT vs. ob-aT (**B**). Gene expression was analyzed using DESeq2 R package. Genes with a *p*-value < 0.01, and a fold change greater than 2 (red color code) and below − 2 (blue color code), respectively, were included. **C** and **D** Volcano plots showing the adjusted *p*-value (adj. $p > 0.05$) for genes differentially expressed between bASCs close to and distant to the breast cancers in lean (**C**) and obese ($p > 0.05$) (**D**) bASCs. Upregulated genes are depicted in red color, downregulated in green, and non-changed genes in blue (adjusted *p*-value > 0.05). **E** and **F** Significantly enriched KEGG pathways (**E**) and GO pathways (**F**) are presented for ln-aT bASCs compared to ln-dT bASCs. For each KEGG or GO pathway, the bar shows the adjusted *p*-value. The numbers (n) behind the pathway names indicate deregulated genes. **G** Violin plots present selected myCAF/iCAF genes differentially expressed. Values reflect the log expression levels of genes from the RNA-seq data. **H** Heatmap depicts significantly differentially expressed cytokine/chemokine genes in four bASCs subgroups. These genes have a fold change greater than 2 (red color code) or below − 2 (blue color code). Genes in (**A**-**F**) have an adjusted *p*-value of ≤0.05 and genes shown in (**G**) have an adjusted *p*-value of ≤0.05, at least for one condition (ln-aT or ob-aT)

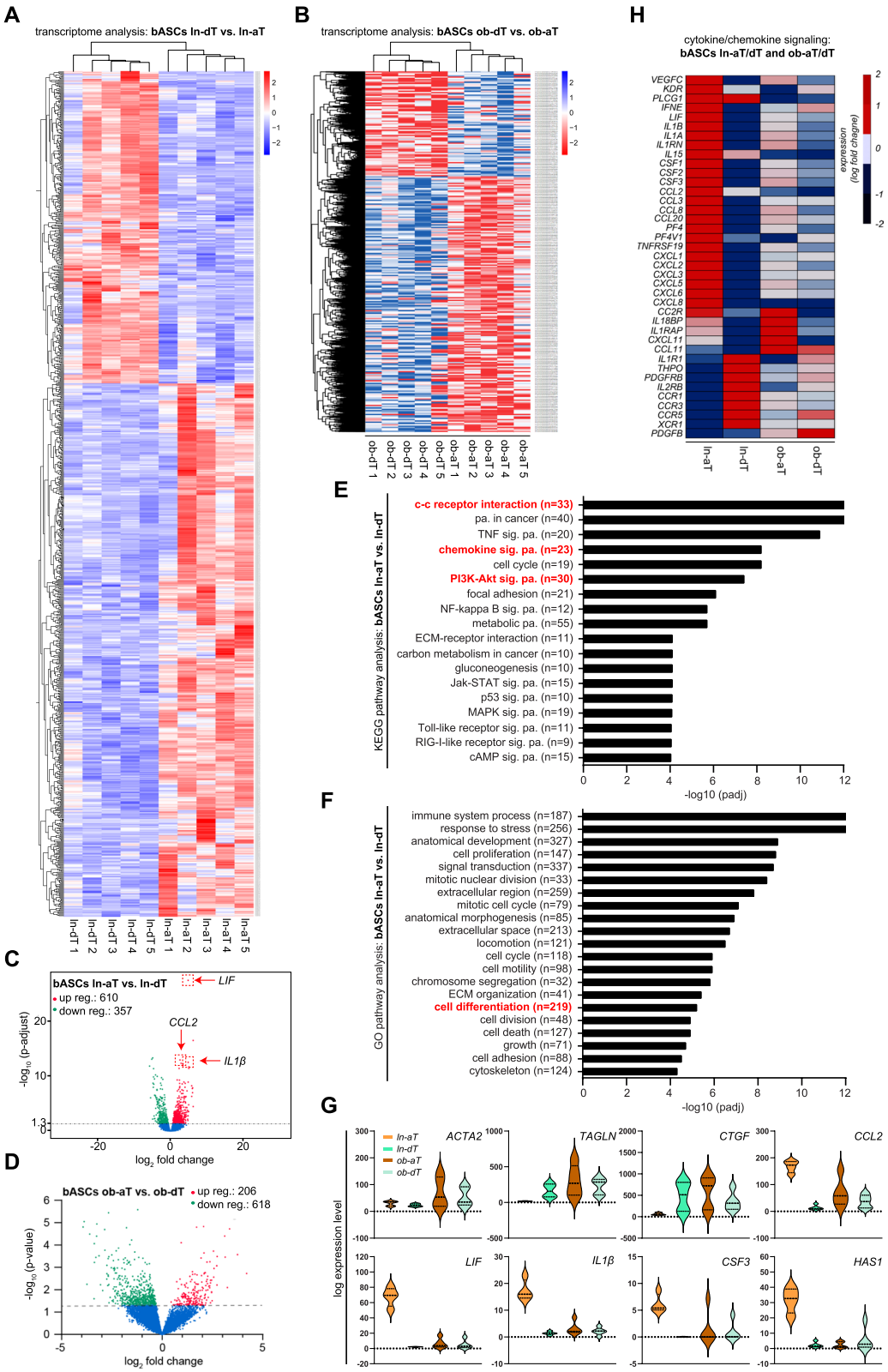

Fig. 3 (See legend on previous page.)

with RQ values of 6.5 to 48.4 in ln-aT bASCs compared to the ln-dT bASCs (Fig. 4A). Remarkably, ob-aT bASCs showed a similar trend with an increased gene expression of *LIF* (RQ: 2.4), *CXCL1* (RQ: 3.0), *CXCL3* (RQ: 2.8), *CCL2* (RQ: 4.5), *FGF1* (RQ: 1.8), FGF2 (RQ: 3.5) and *VEGFC* (RQ: 2.1), but not to the extent of ln-aT bASCs (Fig. 4A). Strikingly, ob-dT bASCs already displayed an enhanced gene expression of *CXCL2*, *CXCL1*, *CXCL3*, *FGF2* and *CCL2,* compared to ln-dT bASCs (Fig. 4A), suggesting a crucial impact of obesity on bASCs.

To examine cytokine secretion, ELISA assays were performed with conditioned media from individual bASC subgroups. IL6 was upregulated in ob bASCs, whereas IL8 was slightly downregulated (Fig. 4B). Both ln-aT bASCs and ob-aT bASCs secreted high levels of cytokines (Fig. 4B). Additionally, ln-aT bASCs, compared to ln-dT bASCs, displayed significantly increased levels of CCL2, CXCL1–3, FGF1, FGF2 and VEGFC (Fig. 4C and D, 1st vs. 2nd bars). As observed by gene analysis (Fig. 4A), ob-aT bASCs also secreted increased levels of CCL2, CXCL1–3 and VEGFC, in comparison to ob-dT bASCs (Fig. 4C and D, 3rd vs. 4th bars), but not to the same extent as ln-aT bASCs did (Fig. 4C and D, 1st vs. 3rd bar).

To corroborate the gene expression data from transcriptomic analysis that suggest an iCAF phenotype for ln-aT bASCs, we analyzed the secretion of inflammatory cytokines and chemokines. Indeed, ln-aT bASCs had significantly increased secretion of CSF3, CXCL10 and IL1β, compared with all three other subgroups (Fig. 4E, 1st to 3rd graphs). Of importance, ob-dT bASCs were highly capable of releasing LIF with a value of 25.4 pg/ml relative to ln-dT bASCs with values of 9.7 pg/ml (Fig. 4E, 4th graph, 2nd and 4th bars), whereas ln- and ob-aT bASCs secreted it in a significantly high amount with 2.4 ng/ml in ln-aT bASCS and 2.2 ng/ml in ob-aT bASCs (Fig. 4E, 4th graph, 1st and 3rd bars). These data underscore the findings from the transcriptome analysis that ln-aT bASCs are de-differentiated into an iCAF-like phenotype. Importantly, most of these cytokines are tumor and metastasis promoting [16, 46, 47], suggesting that one of the main molecular mechanisms how ln/ob-aT bASCs support tumor development is via paracrine signaling.

Ob- and ln-aT bASCs promote the growth of breast cancer spheroids via cell-cell contact

To study the effect of bASCs and their secreted cytokines, spheroids were generated with two luminal B breast cancer cell lines BT474$^{(ER+,\ PR+,\ HER2+)}$ and MDA-MB-361$^{(ER+,\ PR+/-,\ HER2+)}$ [27] and seeded on a bASC feeder layer as indicated in Fig. S3E. Area and diameter of spheroids were measured up to 96 h. The spheroids were then fixed, stained for phospho-histone H3 (pHH3, Ser10), a mitotic marker, α-tubulin and DNA (DAPI), and the mitotic index and cell number were quantified. Low malignant BT474 spheroids, which were grown in a direct co-culture setup on a feeder layer of ln-aT bASCs, showed a growth advantage at 24, 48, 72 and 96 h, compared to a feeder layer formed by ln-dT bASCs (Fig. S4A). The area and diameter were significantly increased in BT474 spheroids, especially at early time points 24 and 48 h (Fig. S4A, C and E). Interestingly, BT474 spheroids co-cultured with ob-aT bASCs displayed an even greater growth advantage compared to ln/ob-dT bASCs (Fig. S4A-F). The direct comparison of lean and obese aT bASCs showed that ob-aT bASCs led to an increased growth rate of BT474 spheroids by 29.97% at 72 h and 27.83% at 96 h compared to ln-aT bASCs (Fig. S5A, black scatter plots), whereas there was no significant difference between lean and obese dT bASCs (Fig. S5A, gray scatter plots). The similar effect was observed for BT474 spheroid diameter, which increased by 18 to 21% over the 72- to 96 h period after co-culture with ob-aT bASCs, compared to ln-aT bASCs (Fig. S5B, black scatter plots). In addition, the diameter of BT474 organoids co-cultured with ob-dT bASCs increased significantly by 13%, compared with ln-dT bASCs (Fig. S5B, gray scatter plots). In line with this, spheroids co-cultured with ob-aT bASCs had a higher cell number and mitotic index than with ln-aT bASCs (Fig. S4G-J, black bars). Only moderate differences were observed on breast cancer cell spheroids co-cultured with lean or obese dT bASCs (Fig. S4G-J, gray bars).

An increased diameter was also observed in MDA-MB-361 spheroids directly co-cultured with aT bASCs (Fig. S5C-J). The growth benefit of spheroids has been further significantly enhanced by co-culture with ob-aT bASCs, compared to ln-aT bASCs (Fig. S5G and H). Like BT474 spheroids, the mitotic index and cell number were also increased in MDA-MB-361 spheroids co-cultured with ob-aT bASCs (Fig. S6A-D, black bars). A moderate promoting effect was observed in the spheroids co-cultured with lean and obese dT bASCs (Fig. S5C-J and S6A-D). These data support previous reports that visceral

(See figure on next page.)

Fig. 4 bASCs adjacent to breast cancer cells have increased gene expression and protein secretion of cancer promoting cytokines. **A** Relative gene levels of *IL6*, *IL8*, *CXCL1*, *CXCL2*, *CXCL3*, *CCL2*, *VEGFC*, *FGF1*, *FGF2*, and LIF are shown for bASC subgroups (ln-dT, ln-aT, ob-dT and ob-aT). The results are from three independent experiments and presented as bar graphs with mean ± SEM. **B**-**E** ELISA assays were performed with conditioned media from bASCs subgroups and the levels of cytokines IL6 and IL8 (**B**), chemokines CXCL1–3 and CCL2 (**C**), growth factors VEGFC and FGF1/2 (**D**), and inflammatory cancer-associated cytokines CSF3, CXCL10, IL1β and LIF (**E**) were analyzed. The results are from three independent experiments and presented as scatter bar graphs with mean ± SEM. Student's t test was used. $*p < 0.05$, $**p < 0.01$, $***p < 0.001$

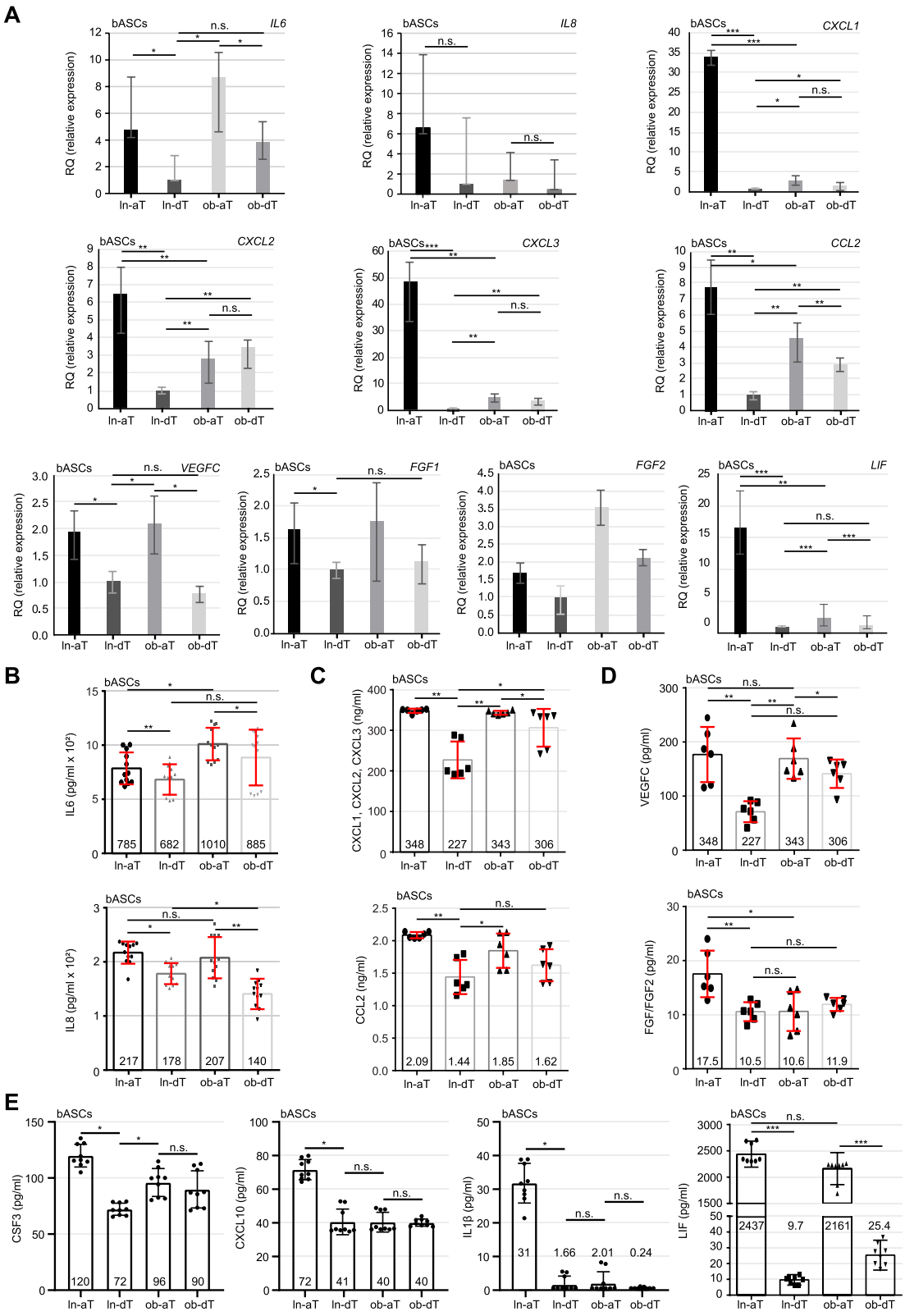

Fig. 4 (See legend on previous page.)

ASCs had a stimulatory effect on cancer cell proliferation in a direct co-culture setup [20, 48]. Collectively, aT bASCs have a highly increased capacity to fuel the growth of low to intermediate malignant breast cancer spheroids, which is further exacerbated by the obese state.

The supernatant of aT bASCs stimulates breast cancer cell motility

A number of chemokines such as CXCL1–3, CXCL10 and CCL2 released from aT-bASCs are known to promote invasion and metastasis [49]. To examine this issue, epithelial MCF7$^{(ER+,\ PR+,\ HER2+)}$ and mesenchymal MDA-MB-231$^{(ER-,\ PR-,\ HER2-)}$ breast cancer cells incubated with supernatants of bASCs were tracked using time-lapse microscopy. The accumulated distance and the velocity of single-tracked cells are commonly used to assess the migratory capacity of cancer cells [50]. Supernatants of both ln- and ob-aT bASCs significantly increased the accumulated distance (ln-aT bASCs: 606 µm; ob-aT bASCs: 615 µm) and the velocity (ln-aT bASCs: 0.90 µm/s; ob-aT bASCs: 0.92 µm/s) of MCF7 cells, compared with control MCF7 cells, which had an accumulated distance of 363 µm and a velocity of 0.54 µm/s (Fig. S6E-G, 1st, 2nd and 4th scatter plots). Consistent with the proliferation results (Fig. S4 and S5), the supernatants of ln/ob-dT bASCs displayed moderate effects on MCF-7 cells with increased accumulated distances of 490 µm and 556 µm (Fig. S6F, 3rd and 5th scatter plots) and increased velocities of 27 to 46% (Fig. S6G, 3rd and 5th scatter plots). No significant impact was observed on the directionality of MCF7 cells (Fig. S6H).

MDA-MB-231 exhibited a significantly higher motility rate, likely due to their invasive mesenchymal phenotype. Non-treated and control medium treated MDA-MB-231 cells demonstrated an accumulated distance of 610 µm and 611 µm, respectively (Fig. S6I and J, 1st and 2nd scatter plots). Notably, the supernatants from ln- as well as from ob-aT bASCs significantly increased the accumulated distance and the velocity of MDA-MB-231 cells (Fig. S6I-K), whereas ln- and ob-dT bASCs had no clear effect on these cells (Fig. S6I-K). Like in MCF7 cells, no obvious effect was observed on the directionality of MDA-MB-231 cells (Fig. S6L). Overall, the data suggest that bASCs stimulate the migratory and invasive capacity of malignant cells, as reported for MSCs [25]. In particular, our results indicate that cancer-educated aT bASCs confer a greatly enhanced ability to promote the motility of low- and high-malignant breast cancer cells, majorly due to their increased secretion of bioactive factors including cytokines and chemokines.

Hybrid spheroids formed with breast cancer cells and bASCs become resistant to tamoxifen and docetaxel

Chemoresistance is a major obstacle in the treatment of breast cancer, and its related molecular mechanisms are not completely understood [10, 51]. To study the roles of bASCs in this aspect, we formed hybrid spheroids consisting of bASCs and low-malignant MCF7$^{(ER+,\ PR+,\ HER2+)}$, BT474$^{(ER+,\ PR+,\ HER2+)}$ or high-malignant MDA-MB-231$^{(ER-,\ PR-,\ HER2-)}$ breast cancer cell lines [27] as displayed in Fig. S7A. These hybrid spheroids were formed with different percentages (85, 70 or 50%, respectively) of breast cancer cells together with 15, 3% or 50% of bASCs. The spheroid area was microscopically measured. MCF7 and MDA-MB-231 breast cancer cells alone showed poor spheroid formation, with an unstructured and unstable phenotype (Fig. S7B-E, 1st scatter plot). The spheroid formation capacity was dramatically increased by adding bASCs (Fig. S7B-E). Hybrid spheroids containing one of the four bASC subgroups significantly increased the spheroid formation, visualized by the area of MCF7 and MDA-MB-231 cells, even with a low concentration of 15% bASCs (Fig. S7B and C, 1st vs. 2nd, 5th, 8th and 11th scatter plots). This observed effect on the spheroid area was enhanced with increasing concentrations of bASCs (15, 30 and 50%) (Fig. S7B and C). In support of the previous results (Fig. S4 and S5), hybrid spheroids formed with ln-aT or ob-aT bASCs were larger than with the control counterparts at all concentrations used (Fig. S7B and C, dark gray vs. light gray scatter plots). The lowest concentration (15%) was chosen for further experiments to mimic breast cancer subtypes with low stroma content [52].

To analyze the impact of bASCs on cancer cell proliferation, *CellTrace*™ tagged MCF7 and MDA-MB-231 spheroids were either cultured with different bASCs supernatants or co-cultured with 15% of bASCs, and the cell count was measured after 96 h by flow cytometry. The control medium did not significantly alter the cell count of MCF7 (Fig. S7F, 1st vs. 2nd boxplot) and MDA-MB-231 cells (Fig. S7G, 1st vs. 2nd boxplot). Moreover, the supernatants of all four bASCs subgroups had no significant impact on the proliferation rate of both cancer cell lines (Fig. S7F and G, 1st to 6th boxplots), except a slight effect of the supernatant from ln-dT bASCs on MDA-MB-231 cells (Fig. S7G, 2nd vs. 4th boxplot). By contrast, MCF7 and MDA-MB-231 spheroids in direct co-culture with bASCs significantly increased their cell numbers (Fig. S7F and G, 2nd vs. 7th–10th boxplots). In further support, both cancer cell lines co-cultured with ln-aT or ob-aT bASCs showed the highest proliferation rates compared to cells co-cultured with control medium (Fig. S7F and G, 2nd vs. 7th and 9th boxplots).

As multiple reports have demonstrated an impact of MSCs on cancer cell chemoresistance [53], we were interested in the potential influence of bASCs on the chemotherapeutic response of breast cancer cells. Hybrid spheroids were formed with BT474 cells (85%) and

bASCs (15%) for 72 h (Fig. S7A). After establishing breast cancer cell (BC)/bASC hybrid spheroids, the spheroids were treated up to 96 h with TMX or docetaxel (DTX), two commonly used chemotherapeutic agents for the treatment of breast cancer patients [54], and their proliferation was measured via cell viability assay. BT474 only spheroids showed a significant growth reduction after 96 h (Fig. 5A), whereas BT474 hybrid spheroids formed with ln-aT or ob-aT displayed no significant growth restriction (Fig. 5B and C), indicating an increased resistance toward both chemotherapeutics. By contrast, hybrid spheroids formed with ln-dT and ob-dT bASCs were still sensitive to the treatment with TMX and DTX, as indicated by significantly reduced cell viability compared with control cells treated with DMSO (Fig. S8A and B). These data were further supported by MCF7 and MDA-MB-231 hybrid spheroids. Both cell lines were sensitive to each chemotherapeutic agent (Fig. S8C and H) and lost this sensitivity upon integration of ln-aT or ob-aT bASCs into the spheroids (Fig. S8E, G, J and L). Similar to BT474 cells, MCF7 and MDA-MB-231 spheroids co-cultured with ln-dT and ob-dT bASCs failed to mediate this resistance (Fig. S8D, F, I and K). In conclusion, integration of ln- or ob-aT bASCs prevented apoptosis induction by chemotherapeutic agents in breast cancer spheroids, in contrast to control dT bASCs.

We next analyzed DTX-induced DNA damage and repair in BT474 hybrid spheroids. Spheroid cells were treated with 50 nM of DTX for 72 h, stained for DNA damage markers γ-H2AX (Ser139) and p53-binding protein 1 (53BP1) [55], and three parameters were examined microscopically: double positive cells, cells with 20 or more double positive foci and the overall foci count. As indicated by the growth reduction in the cell viability assay (Fig. 5A), prolonged treatment with DTX induced massive DNA damage in BT474 cells showing a double positive staining in 72–73% of control cells or cells incubated with control medium (Fig. 5D and G, 3rd and 4th bars), 15–16% of cells had 20 or more foci (Fig. 5E, 3rd and 4th bars), and the overall foci count was 20–22 foci per cell (Fig. 5F, 3rd and 4th scatter plots). Both ln- or ob-aT bASC integrated spheroids displayed a similar trend, the number of double positive cells decreased to 39–51% (Fig. 5D and G, 5th and 7th bars), the percentage of cells with ≥20 foci turned down to 4–5% (Fig. 5E, 5th and 7th bars), as well as the foci per cell was reduced to 8–9 (Fig. 5F and G, 5th and 7th scatter plots). The control ln- and ob-dT bASCs were not able to reduce the percentage of positive cells or cells with more than 20 foci in hybrid spheroids (Fig. 5D, E and G, 6th and 8th bars). Only the absolute number of foci was slightly decreased to 18–19 per cell (Fig. 5F, 6th and 8th scatter plots). To further corroborate these data, BT474 hybrid spheroids were labelled with a live (calcein-490 nm/515 nm)/dead (propidium iodide-535 nm/617 nm) marker and treated with TMX (5 µM) or DTX (50 nM) for up to 3 days. The cell surface area and the ratio between live/dead fluorescent signals were analyzed microscopically. In control cells, both chemotherapeutic agents induced apoptosis, indicated by a robust increase in the dead fraction of cells and a decreased cell surface area (Fig. 5H-L, 1st to 3rd bars). Interestingly, BT474 cells, which were reported to display moderate resistance to TMX [56], showed indeed a modest apoptosis induction compared to DTX-treated cells (Fig. 5H-L, 2nd vs. 3rd bars). Consistent with these observations, the cell surface area of BT474/ln/ob-aT bASC hybrid spheroids was not significantly reduced after TMX or DTX treatment (Fig. 5H, I and L) and had a lower live/dead ratio compared with BT474 control cells (Fig. 5J, K and L). In contrast, both ln/ob-dT bASCs only marginally reduced apoptosis induction, as evidenced by slightly decreased fluorescent intensity of propidium iodide and reduced cell surface area (Fig. 5H-L). Taken together, these results imply the potential clinical significance of bASCs in inducing chemoresistance in breast cancer cells. These results provide evidence that a high number of aT bASCs in the TME may influence the response to chemotherapy in primary breast cancer.

Transcriptomic changes in breast cancer cells induced by lean and obese bASCs

To investigate the crosstalk between bASCs and BC cells (BT474 and MDA-MB-231) at the molecular level, both cell types were grown in direct co-culture (85% BCs / 15%

(See figure on next page.)

Fig. 5 Hybrid spheroids of breast cancer cells and ln-aT/ob-aT bASCs demonstrate an increased resistance to chemotherapeutic agents. **A**-**C** BT474 spheroids (**A**), BT474/ln-aT bASCs (**B**) and BT474/ob-aT bASCs (**C**) hybrid spheroids, generated for 24 h, were transferred into 96-well low attachment plates, treated with DMSO, TMX (5 µM) or DTX (50 nM) for up to 96 h. Cell viability was measured at indicated time points. The results are based on three independent experiments and presented as mean ± SEM. **D**-**G** Indicated spheroids were treated with 50 nM DTX for 72 h, stained for DNA damage markers γ-H2AX (red) and 53BP1 (green), and DNA (DAPI, blue). **G** Representatives are shown. White arrows indicate cell nuclei with 20 ≥ foci. Scale: 25 µm. D-F Quantification of γ-H2AX and 53BP1 double positive cells (**D**, $n = 15$ fields in each group), cells with 20 ≥ foci (**E**, $n = 15$ fields in each group) and double positive foci per cell (**F**, $n = 90$ cells in each group). **H**-**L** BT474- and hybrid spheroids were stained using the live/dead viability/cytotoxicity kit. Spheroid surface area (**H** and **I**, $n = 7$–11 fields in each group), and the ratio between the fluorescence intensity of viable cells (calcein/green) and the dead fraction (PI/red) (**J** and **K**, $n = 7$–12 fields in each group) were evaluated. The results are based on three independent experiments and presented as mean ± SEM. **L** Representative images of spheroids treated with DTX (50 nM) for 72 h are shown. White dotted lines depict the measured area of the spheroids. Scale: 250 µm. Student's t test was used in (**A**-**C**). Unpaired Mann-Whitney U test was used in (**D**-**F**) and (**H**-**K**). *$p < 0.05$, **$p < 0.01$, ***$p < 0.001$

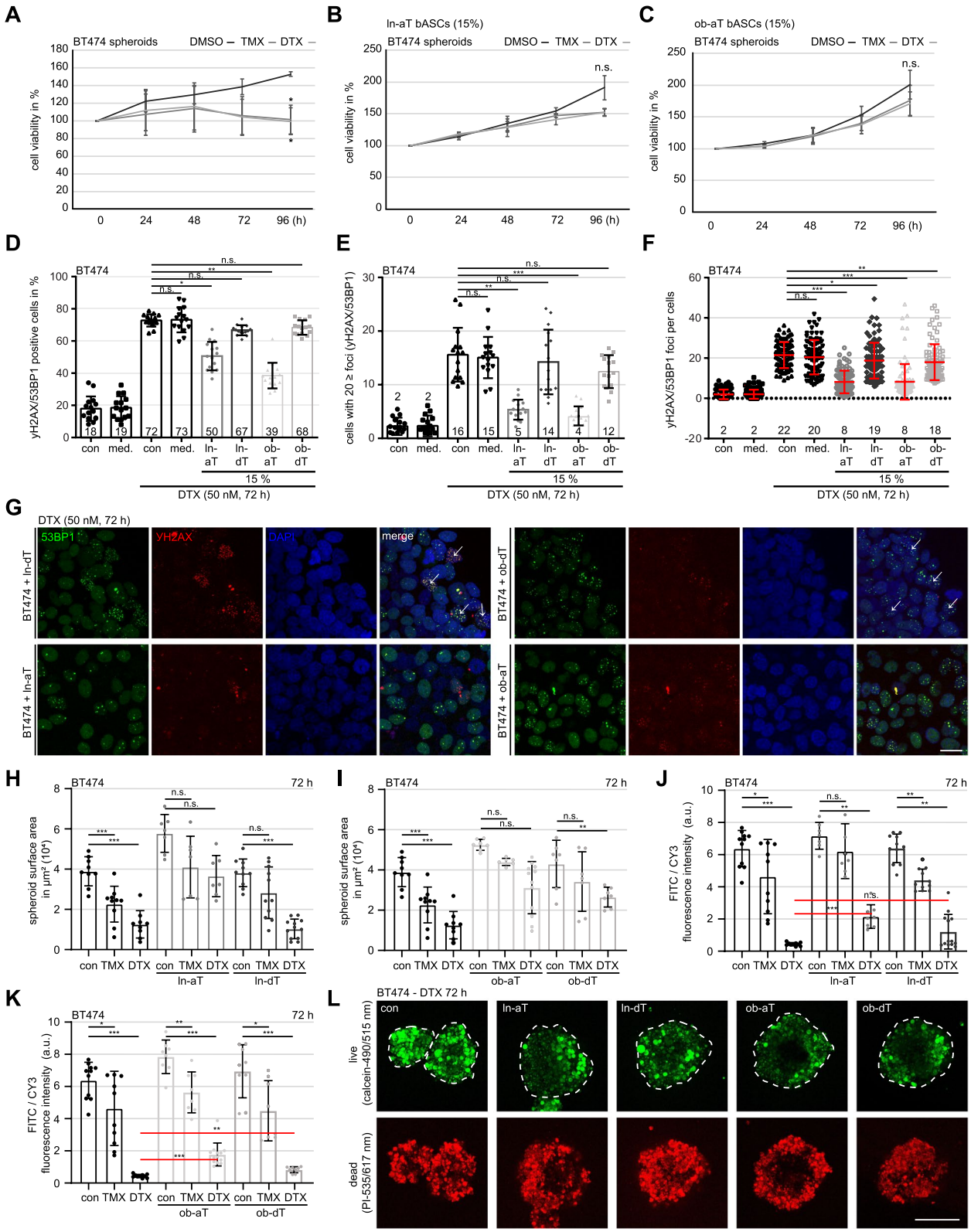

Fig. 5 (See legend on previous page.)

bASCs), as in experiments with hybrid spheroids. After 14 days of direct co-culture, the cells were sorted using the classical MSC markers CD90, CD73 and an epithelial marker CD24 (Fig. S8M). Total RNAs were extracted from sorted BC cells for transcriptomic mRNA-sequencing. The RNA-seq data revealed that the direct co-culture with bASCs had a huge impact on both breast cancer cell lines. Co-cultured and sorted BCs had several hundred deregulated (up- and downregulated) genes displayed by volcano plots (Fig. 6A and S9A). Strikingly, co-cultured with ln-aT bASCs induced 16.6-fold more deregulated genes in BT474 cells and 17.8-fold more in MDA-MB-231 cells compared to these cells co-cultured with ln-dT bASCs (Fig. 6A and S9A, 1st vs. 2nd volcano plot). A similar trend of increased up- or downregulated genes could be observed in both BC lines co-cultured with ob-aT bASCs, but not to the same extent as in BC lines co-cultured with ln-aT bASCs (Fig. 6A and S9A, 1st vs. 3rd volcano plot). The GO pathway enrichment analyses revealed that at least three key pathways were affected in BT474 cells by co-culturing with ln-aT bASCs: regulation of cell migration, cell growth and EMT (Fig. 6B). The RNA-seq data for BT474 cells in direct co-culture with ob-aT bASCs were diverse, nevertheless suggesting gene changes in cell cycle progression, cellular metabolism, cellular stress, and apoptosis response (Fig. 6C).

Moreover, heatmaps were generated for the most interesting significant genes involved in cell motility and migration (Fig. 6D), DNA repair and apoptosis (Fig. 6E), and cell cycle regulation (Fig. 6F). Intriguingly, BT474 cells co-cultured with ob-aT bASCs presented an entirely different gene profile (Fig. 6D-F, 4th row), whereas these cells directly co-cultured with ln-aT, ln-dT or ob-dT bASCs had many overlapping genes that were deregulated in the same direction (Fig. 6D-F, 2nd, 3rd and 5th rows). This is in accordance with multiple reports highlighting a general tumor-promoting effect of MSCs co-cultured with BC cell lines [57]. The common pattern of breast cancer cells co-cultured with ln-aT, ln-dT or ob-dT bASCs indicated a changed expression of important cytoskeleton genes *RAC2* and *VIM*, ECM genes *LAMC2* and *ICAM1*, DNA repair genes *ATM* and *BIRC2–3,* and cell cycle regulating genes *CCNA1*, *CCND2* and *CENPE* (Fig. 6D-F, 2nd, 3rd and 5th row), allowing possible molecular explanations for the increased cell proliferation, motility and chemoresistance observed in the experiments (Fig. 5 and Fig. S4–8). BT474 cells directly co-cultured with ob-aT bASCs altered their transcriptomic profile to a great extent (Fig. 6D-F, 4th row). These co-cultured cells upregulated ECM related genes such as *ITGA1* and *LAMC2*, but downregulated cytoskeleton associated genes including *RAC2* and *VIM* (Fig. 6D, 4th row), suggesting a completely different molecular mechanism for the observed enhanced cell motility (Fig. S6E-J). Despite downregulation of most DNA repair and apoptosis genes, *ATM* was significantly upregulated ($p < 0.001$), together with *MYCN*, an important DNA damage response gene (Fig. 6E, 4th row) [58]. In line with the increased proliferation induced by direct co-culture with ob-aT bASCs (Fig. S4 and 5), many regulatory genes of the cell cycle checkpoint were downregulated, including *BUB3*, *CHEK1–2* and *MAD2L1–2* (Fig. 6F, 4th row) [59].

MDA-MB-231 cells directly co-cultured with ln-aT bASCs displayed deregulated genes in crucial signaling pathways including *PI3K*, *MAPK*, *RAS*, *mTOR*, *TNF*, *ERBB* and *VEGF* (Fig. S9B). Whereas MDA-MB-231 cells co-cultured with ob-aT bASCs affected signaling pathways involved in the cell cycle, apoptosis, DNA repair and TGFβ signaling (Fig. S9C). Distinct from BT474 cells, MDA-MB-231 co-cultured with each of four bASC subgroups presented an upregulated gene expression of various cell cycle regulators such as *CCNE2*, *WEE1*, *AURKA*, consistent with the proliferation data (Fig. S9D). MDA-MB-231 cells co-cultured with ln-aT bASCs had a decreased expression of multiple inflammatory and apoptotic genes such as *CASP1*, CASP4–5 and *CASP7–10,* and an increased expression of various cell survival genes including *MYCN*, *KRAS* and *BCL2* (Fig. S9E, 2nd row). By contrast, MDA-MB-231 cells co-cultured with ob-aT bASCs did not affect the mentioned caspases, but enhanced the gene expression of c-*MYC*, *FOS*, *BCL2* and *BCL2A1* (Fig. S9E, 4th row). Cancer stem cells (CSC) are

(See figure on next page.)

Fig. 6 Transcriptome profiles of triple positive BT474 cells directly co-cultured with bASCs. **A**-**F** BT474 cells cultured for 14 days alone or in direct co-culture with different bASCs (ln/ob-dT/aT) were sorted for RNA-seq analysis ($n = 3$). The gene expression was analyzed using DESeq2 R package. **A** Volcano plots show the adjusted *p*-value for genes differentially expressed between control BT474 cells and BT474 cells directly co-cultured with ln-aT bASCs (1st volcano plot), ln-dT bASCs (2nd volcano plot), ob-aT bASCs (3rd volcano plot) and ob-dT bASCs (4th volcano plot). **B** and **C** GO enrichment analysis of RNA-seq data with a *p*-value ≤0.05. Gene count: the number of genes that are deregulated in the pathway. Gene ratio: ratio of the number of target genes divided by the number of all genes in each pathway. Significance is color coded as indicated (high *p*-value, red; low *p*-value, blue). **D**-**F** Heatmaps of deregulated genes involved in motility and migration (**D**), DNA repair and apoptosis (**E**), and cell cycle regulation (**F**). A fold change of ≥2 (red color code) and ≤ − 2 (blue color code) are shown. Included genes have a *p*-adjusted value of ≤0.05 for at least one condition (ln-aT or ob-aT)

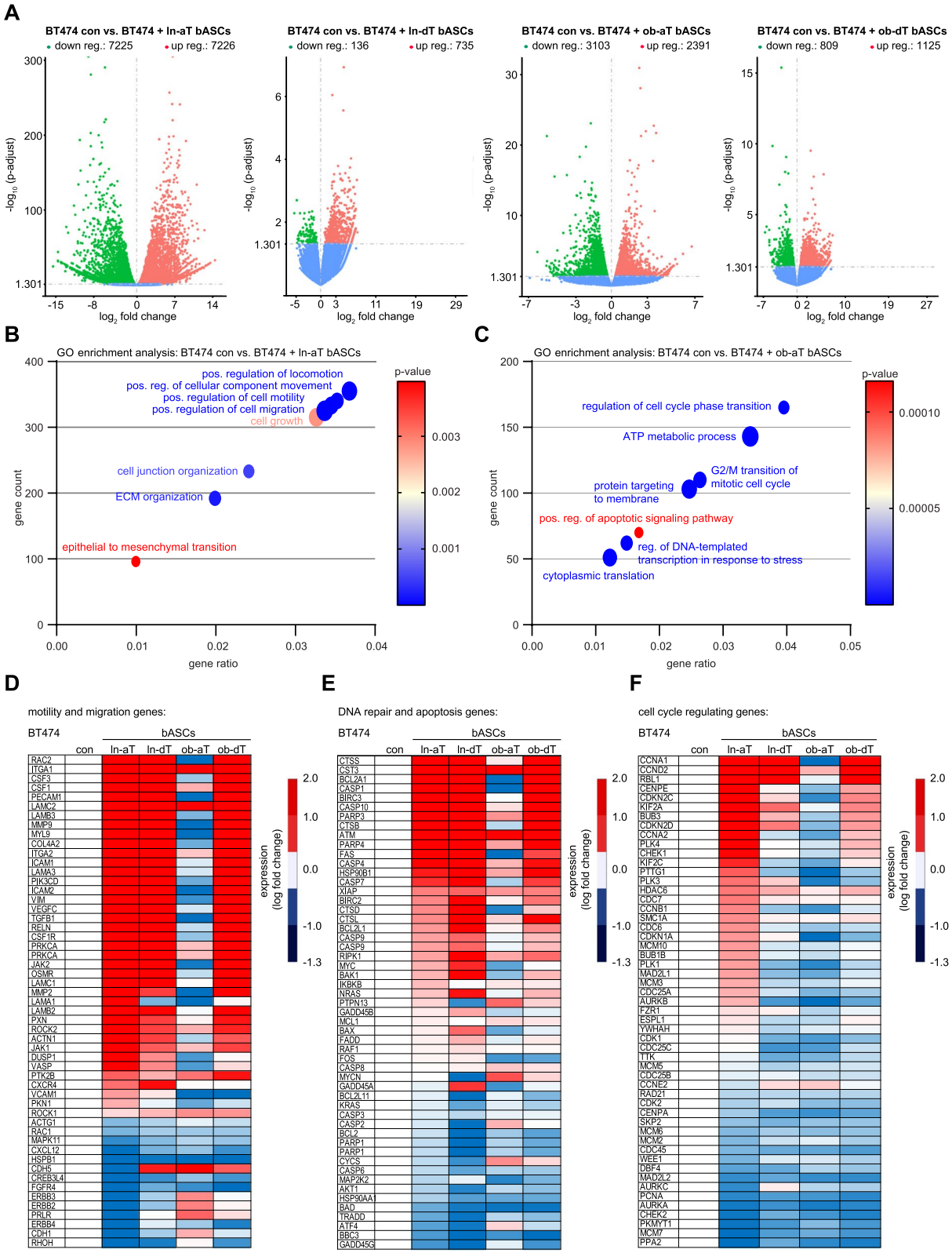

Fig. 6 (See legend on previous page.)

often associated with an increased drug resistance [60]. To look at this issue, a heatmap was generated with genes concerning stemness in MDA-MB-231 cells (Fig. S9F). The genes of stem cell markers such as *ALDH2*, *BCL2*, *WEE1*, *TP63* and *SOX2* were upregulated in these cells co-cultured with each of aT bASCs (Fig. S9F, 2nd and 4th rows). Additionally, MDA-MB-231 cells co-cultured with ob-aT bASCs also overexpressed *ALDH1A1* and *KLF4* (Fig. S9F, 4th row). In conclusion, direct co-culture with aT bASCs had a major impact on the transcriptomic profile of low- as well as high-malignant breast cancer cells by greatly altering the expression of crucial genes associated with the cell cycle, DNA repair and motility.

Both aT bASC subtypes trigger the EMT in epithelial breast cancer cells and increase cancer stem cell markers in mesenchymal breast cancer cells

The involvement of the EMT in drug resistance is well documented both in vitro as well as in vivo [61]. To address this, the deregulated EMT related genes (Fig. 6B) were further analyzed. As depicted by the violin plots, BT474 cells co-cultured with ln-aT bASCs highly upregulated the gene expression of EMT transcriptional factors including *ZEB1*, *TWIST1*, *SNAI1* and *SNAI2*, with an associated increase of *VIM* as well as a decrease of *CDH1* (Fig. 7A, 2nd violin plot). Though in a similar pattern, BT474 cells co-cultured with ob-dT bASCs displayed a reduced extent compared to ln-aT bASCs (Fig. 7A, 2nd, 3rd and 5th violin plots). Co-culture with ob-aT bASCs had hardly an effect on EMT related genes in BT474 cells (Fig. 7A, 4th violin plot). Intriguingly, the mesenchymal MDA-MB-231 cells co-cultured with bASCs displayed minor changes in EMT-related genes and co-culture of ob-aT bASCs even downregulated gene levels of *ZEB1*, *SNAI1*, *SNAI2* and *VIM*, together with an increased gene expression of *CDH1* (Fig. 7A, 1st vs. 4th violin plot). To corroborate these RNA-seq data, we performed qPCR analyses with sorted BT474 cells directly co-cultured with different bASCs for 14 days. Indeed, the qPCR results demonstrated an EMT induction in the BT474 cells (Fig. 7B). The ln-aT bASCs affected significantly the EMT related genes by upregulating *ZEB1*, *TWIST1*, *SNAI1*, *SNAI2* and *VIM* (Fig. 7B, graph 1 to 5, 2nd rows). *EPCAM*, an important epithelial marker, was downregulated in these cells (Fig. 7B, graph 6, 2nd row). In addition, two other genes indirectly involved in the EMT, *STAT3* as well as *BCL6,* were also upregulated (Fig. 7B, graph 7 and 8, 2nd row). Interestingly, BT474 cells co-cultured with each of the subgroups (ln/ob-dT and ob-aT) presented a similar tendency with increased gene expression of *SNAI1, SNAI2, VIM*, *STAT3* and *BCL6,* and a decreased level of *ECPAM* (Fig. 7B).

The combined mRNA data from qPCR and RNA-seq were further corroborated with immunofluorescence staining of E-cadherin, an epithelial marker, and N-cadherin, a mesenchymal marker, in BT474 and MCF7 cells indirectly co-cultured with bASCs subgroups. The results showed that ln-aT bASCs were able to significantly increase the size of MCF7 and BT474 cells (Fig. S10A, B and E), which is a direct consequence of reduced apical-basal polarity. In line with this observation, the co-culture with ln-aT bASCs reduced the E-cadherin signal, whereas the N-cadherin signal was drastically increased (Fig. S10A-G). All other bASC subgroups (ln-dT, ob-dT and ob-aT) were able to partly induce EMT in MCF7 and BT474 cells, but to a less extent compared to ln-aT bASCs (Fig. S10A-D). These results underscore the notion that ln-aT bASCs are the most potent subgroup to induce the EMT in breast cancer cells (Fig. S10A-G).

MDA-MB-231 cells co-cultured with bASCs exhibited barely any change in the expression of EMT-related genes (Fig. 7A, lower panel). Instead, as shown in the heatmap (Fig. S9F), multiple CSC-associated genes were affected in the transcriptome data (Fig. 7C). These included the upregulation of classical CSC genes *c-MYC*, *ALDH1A1*, *ALDH2*, *KLF4, CD34, CD90, CXCR5* and *LGR5* [62], as well as genes involved in pluripotency including *SOX2*, *SOX9*, *BCL2* and *GATA3* (Fig. 7C). To corroborate these data, we performed qPCR with the same sorted MDA-MB-231 cells. These cells demonstrated indeed significantly increased *NANOG, OCT4, SOX2, SOX9* and *BCL6*, moderately elevated c-*MYC* and *KLF4*, and reduced *BCL2* gene levels (Fig. 7D and Fig. S10H). Particularly, ob-aT bASCs triggered the CSC gene expression

(See figure on next page.)

Fig. 7 ln-aT bASCs induce the EMT in BT474 cells, whereas ob-aT bASCs stimulate MDA-MB-231 cells into a CSC phenotype. **A** and **C** BT474 and MDA-MB-231 cells were directly co-cultured with different bASCs (ln-aT, ln-dT, ob-aT and ob-dT) and were sorted for RNA-seq. Three independent experiments were performed for this analysis. **A** Representative violin plots show selected EMT marker genes. Values represent the log expression levels of genes from the RNA-seq data. Included genes have an adjusted *p*-value of ≤0.05 for at least one condition (ln-aT or ob-aT). **B** Relative levels of EMT-associated genes, including *TWIST1*, *ZEB1*, *SNAI1*, *SNAI2*, *VIM*, *EPCAM*, *STAT3* and *BCL6*, are shown for different bASC subgroups (ln-dT, ln-aT, ob-dT and ob-aT). The results are from three independent experiments and presented as bar graphs with mean ± SEM. **C** Representative violin plots show selected CSC marker genes. Values represent the log expression levels of genes from the RNA-seq data. Included genes have an adjusted *p*-value of ≤0.05 for at least one condition (ln-aT or ob-aT). **D** Relative gene levels of CSC-associated genes c-*MYC*, *OCT4*, *SOX2* and *BCL6* are shown for different bASC subgroups (ln-dT, ln-aT, ob-dT and ob-aT). The results are from three independent experiments and presented as bar graphs with mean ± SEM. Student's t test was used. *$p < 0.05$, **$p < 0.01$, ***$p < 0.001$

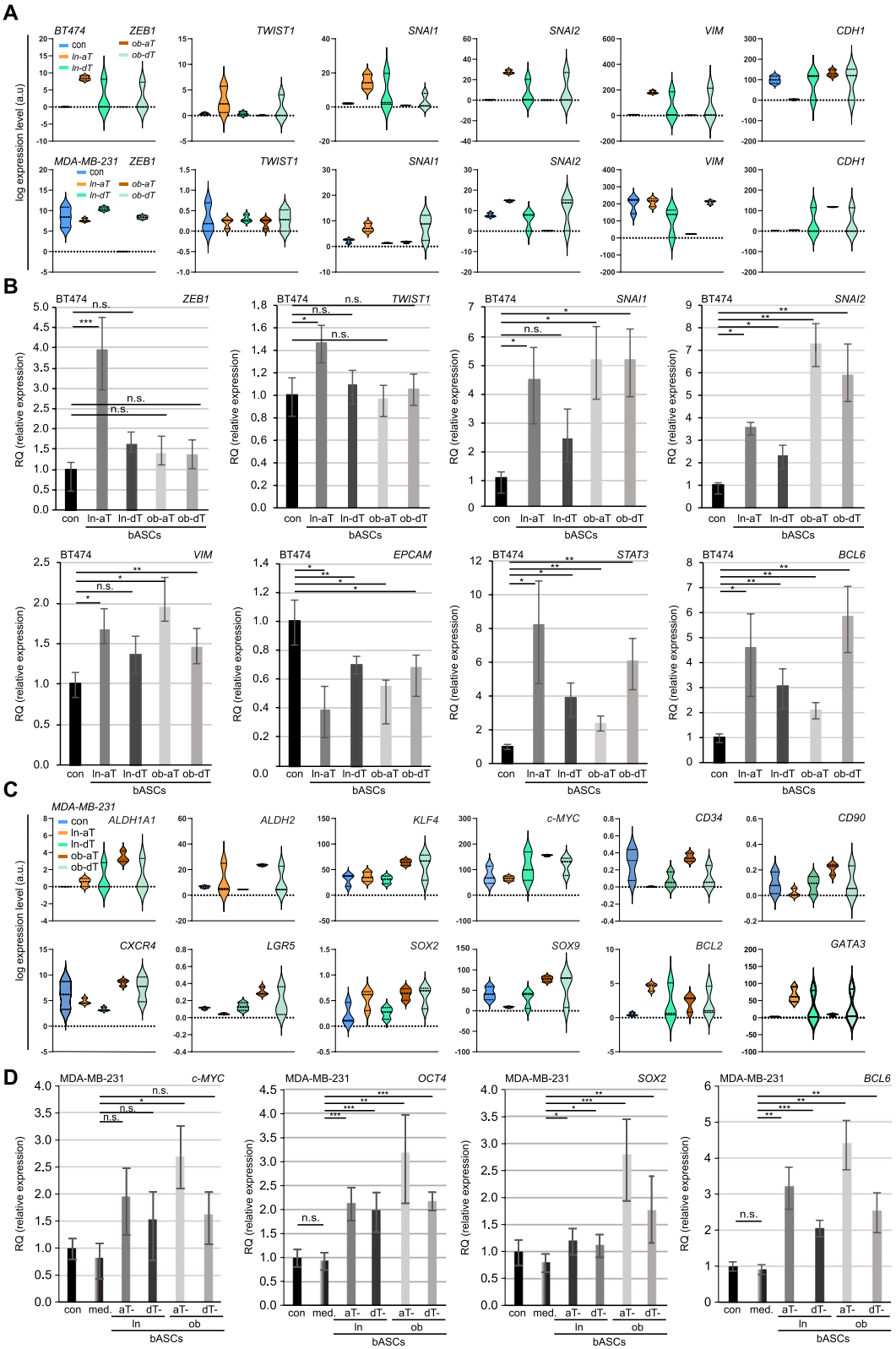

Fig. 7 (See legend on previous page.)

more strongly than ln-aT bASCs in MDA-MB-231 cells (Fig. 7D and Fig. S10H, 3rd vs. 5th bar). In sum, the results highlight an immense impact of bASCs on the transcriptome profile of breast cancer cells. Specifically, ob-aT bASCs induce a more CSC-like phenotype in highly malignant mesenchymal MDA-MB-231 cells.

The expression of LIF and αSMA in the cancer tissue stroma correlates with BMI of breast cancer patients

To address if BMI of the breast cancer patients could be related to the de-differentiation processes in the breast cancer tissue, as indicated in Table S4, 32 breast cancer samples classified as T3/T4 from 16 lean- (BMI ≤ 25) as well as from 16 patients with obesity (BMI ≥ 35) were stained for LIF (iCAF) and αSMA (myCAF) by immunochemistry and evaluated with the weighted score [63]. Although both staining showed no significant changes in the breast cancer cell population (Fig. 8A-E), the tumor stroma displayed a significant correlation between BMI and both stained proteins (Fig. 8A-E). The weighted score for the αSMA staining was increased from 5.5 in lean patients to 10.7 in obese patients (Fig. 8A, B and E). On the contrary, the LIF staining was increased in lean patients with 5.3 compared to 3.6 in patients with obesity (Fig. 8C-E). These data point to the notion that the breast cancer stroma is significantly affected by BMI of breast cancer patients, with crucial consequences for the phenotype and expression profile of the TME cells including bASCs.

Discussion

Despite intense research, questions remain regarding the relationship and interaction between MSCs/ASCs and malignant cells. There are various reports suggesting tumor-promoting effects on the one hand and tumor-inhibiting functions on the other hand [53, 57, 64]. In the present work, we show close reciprocal exchange between bASCs of the TME and breast cancer cells. This crosstalk leads to transcriptomic changes in bASCs that in turn fuel malignancy of breast cancer cells. These findings are achieved by employing bASCs from mammary adipose tissue distant and adjacent to breast cancers of the same patient, distinguishing this study from other investigations that used MSCs of non-mammary origins [20, 65], only tumor adjacent cells [66, 67] or "cancer-educated" MSCs [68]. The observed de-differentiation of bASCs is of particular significance. bASCs near breast cancers from lean patients adopt an inflammatory cancer-educated phenotype, whereas obesity mainly leads to the development of a myofibroblastic cancer-associated phenotype in vitro and ex vivo. By cytokine/chemokine secretion and direct cell-cell contact, both cancer-educated bASCs closely communicate with breast cancer cells and other components of the TME, thus reinforcing the malignancy of breast cancer.

We show that aT bASCs significantly reduce their ability to differentiate into all three aforementioned lineages, in accordance with a previous study reporting a reduced adipogenic differentiation capacity of ASCs from the breast cancer TME [69]. RNA-seq data provide several possible molecular explanations. First, compared to their counterparts ln-dT bASCs, 219 differentiation-related genes were significantly deregulated in ln-aT bASCs including the upregulated genes *ERBB4*, *ROBO2* and *SLIT2*. *ERBB4* is known to promote proliferation in aged MSCs via activating the PI3K/AKT and MAPK pathways [70]. The overexpression of secreted glycoprotein ligand SLIT2 and its immunoglobulin receptor ROBO2 are associated with reduced osteogenic differentiation in rat and murine mesenchymal progenitor cells [71]. Second, the transcription factor *E2F1*, known for its essential role of controlling stem cell fate by regulating the transcription of key cell cycle regulators cyclin A/D/E in various stem cell lineages [72, 73], is upregulated in ln-aT. Indeed, the genes *CCND1*, *CCND3* and *CCNE1* were significantly upregulated in ln-aT bASCs compared to their distant counterparts. Of importance, like ln-aT bASCs, ob-aT as well as ob-dT bASCs display enhanced *E2F1*. ob-dT bASCs differentiate less efficiently than ln-dT bASC, strengthening the negative impact of obesity on the differentiation capacity of MSCs in various adipose tissue types [9, 74]. These data highly suggest that the TME renders bASCs to a more actively proliferating phenotype, whereas genes and pathways responsible for differentiation are downregulated.

(See figure on next page.)

Fig. 8 Increased αSMA and LIF in the cancer stroma from obese and lean patients, respectively. **A** and **C** Formalin-fixed and paraffin-embedded (FFPE) T3/4 breast cancer tissue sections of lean (BMI ≤ 25) or obese (BMI ≥ 35) patients were immunohistochemically stained with LIF (**C**) or αSMA (**A**) antibody (brown), respectively, and counterstained with hematoxylin (blue). Scale: 100 µm. Inset I and II scale: 50 µm. **B** and **D** Quantification of the weighted score in breast cancer cells and tumor stroma for LIF (**D**) and αSMA (**B**). The results are presented as bar and scatter plots showing the mean value ± SEM ($n = 32$, 16 lean / 16 obese breast cancer tissues). Student's t test was used. *$p < 0.05$, ***$p < 0.001$. **E** Table depicts LIF and αSMA staining intensity, percentage of positive tumor stroma and weighted score in 32 breast cancer tissue sections. **F** Schematic illustration of the proposed working model. The breast cancer TME has a crucial impact on the properties of bASCs and on their cell-cell interaction capacity. The de-differentiation process within the TME is highly dependent on the cellular context and is influenced by BMI of patients. Both cancer-educated bASCs phenotypes, iCAF and myCAF, have drastic impacts on breast cancer cells, leading to different tumor promoting profiles in low and high malignant cancer cells

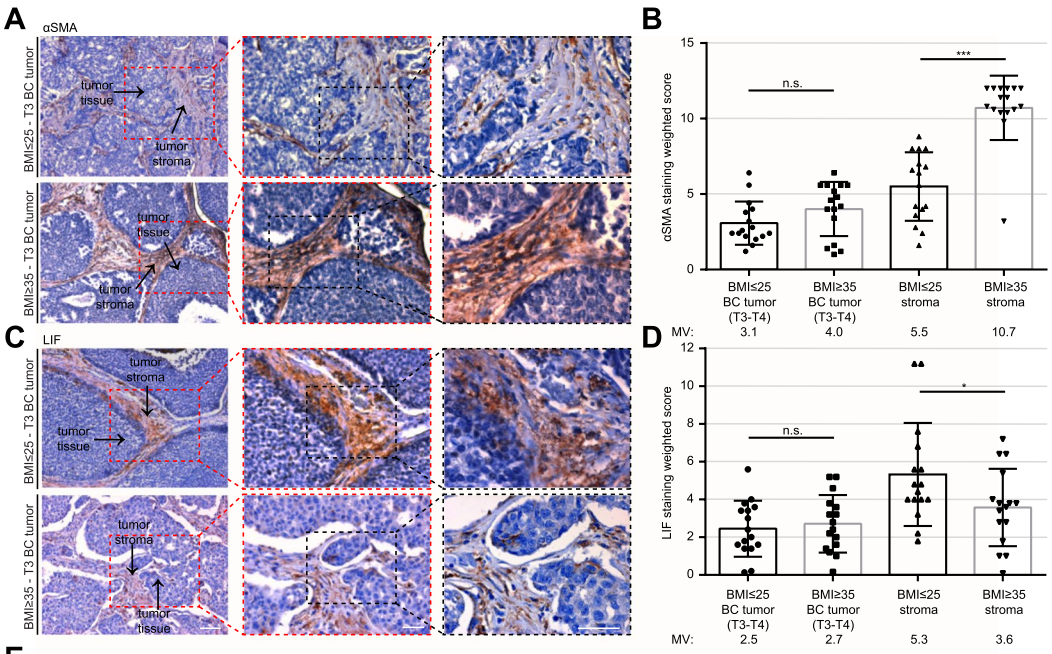

E αSMA and LIF staining intensity, percentage of positive stroma cells and the weighted score in 32 patients with breast tumors (T3-T4).

Protein/BMI	Staining intensity n (%)		% positive stroma cells n (%)		Weighted score	
αSMA/ BMI≤25	Weak Moderate Intense	5 (31.25) 11 (68.75) 0 (0.00)	0-25 26-50 51-75 >75	1 (6.25) 4 (25.00) 4 (25.00) 7 (43.75)	1-3 (low) 3-6 (moderate) 6-12 (high)	3 (18.75) 6 (37.50) 7 (43.75)
αSMA/ BMI≥35	Weak Moderate Intense	1 (6.25) 1 (6.25) 14 (87.50)	0-25 26-50 51-75 >75	0 (0.0) 1 (6.25) 0 (0.0) 15 (92.875)	1-3 (low) 3-6 (moderate) 6-12 (high)	1 (6.25) 0 (0.00) 15 (92.875)
LIF/ BMI≤25	Weak Moderate Intense	12 (75.00) 2 (12.50) 2 (12.50)	0-25 26-50 51-75 >75	0 (0.0) 2 (12.50) 1 (6.25) 13 (81.25)	1-3 (low) 3-6 (moderate) 6-12 (high)	3 (18,75) 9 (56.25) 4 (25.00)
LIF/ BMI≥35	Weak Moderate Intense	14 (87.50) 1 (6.25) 1 (6.25)	0-25 26-50 51-75 >75	3 (18,75) 1 (6.25) 5 (31.25) 7 (43.75)	1-3 (low) 3-6 (moderate) 6-12 (high)	6 (37,50) 7 (43,75) 3 (18,75)

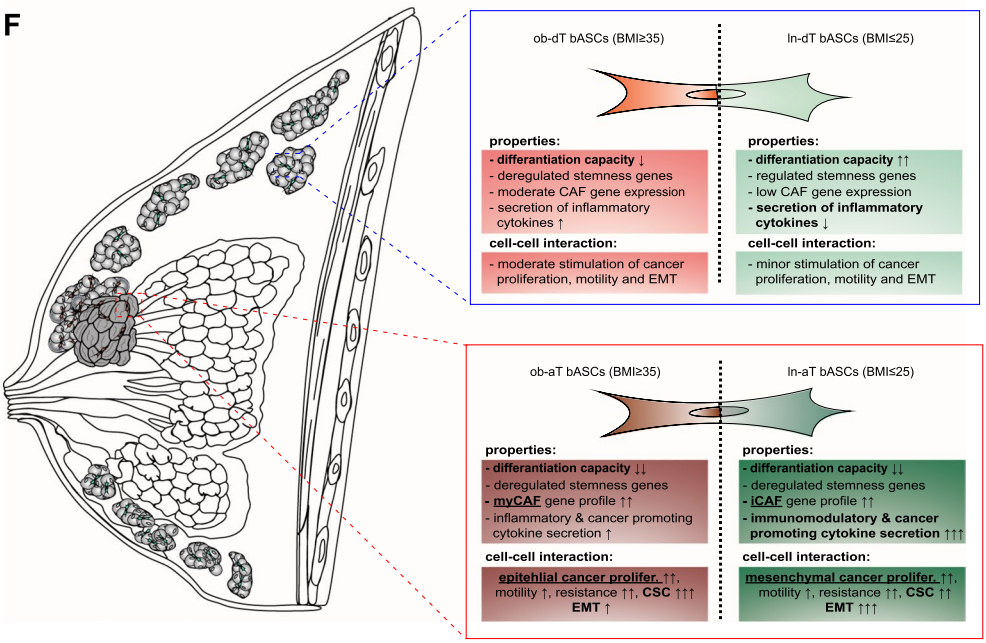

Fig. 8 (See legend on previous page.)

Another explanation for the reduced differentiation capacity is the de-differentiation of bASCs into cancer-associated phenotypes, demonstrated by the changed transcriptome profiles, which mostly resemble CAF-like signatures in the TME [38]. Recent approaches such as RNA-seq, proteomics and single-cell sequencing have revealed several CAF subtypes with specific gene signatures and specialized tumor promoting functions [16, 38, 47]. The two most prominent populations are myCAFs and iCAFs. While myCAFs, characterized by high expression of *αSMA*, *TAGLN*, *CTGF* and *FAP*, are involved in ECM remodeling, promoting cancer cell migration, invasion and therapy resistance [40, 75, 76], iCAFs, classified by expression of cytokine genes including *LIF*, *IL1β*, *CSF3*, *CXCL10* and *CCL2*, exert immunosuppressive and tumor growth promoting functions in the TME [38, 40, 77]. Interestingly, ln-aT bASCs more closely resemble an iCAF phenotype associated with high secretion of immunomodulatory cytokines, whereas ob-aT bASCs are more similar to myCAFs, underscoring a significant impact of obesity on bASC de-differentiation. These findings are in accordance with a previous study showing that ASCs from obese patients were more prone to take over a myCAF-like phenotype after direct co-culture with low-malignant cancer cells [78]. This could be explained by chronic inflammation and increased inflammatory cytokines in the obese state, which are known to "activate" fibroblasts and stimulate the expression of αSMA [78, 79]. These data provide evidence that the TME is capable of reducing the differentiation capability of bASCs and instead ob-aT bASCs and ln-aT bASCs into cancer-educated myCAFs and iCAFs, respectively, which further fuel cancer progression via different molecular signaling pathways.

Despite the differences observed in the RNA-seq analyses, both ln- and ob-aT bASCs significantly increase proliferation, spheroid formation, and motility of breast cancer cells. Surprisingly, compared to ob-aT bASCs, ln-aT bASCs are less efficient in stimulating the proliferation of epithelial-like breast cancer cell lines BT474, MCF7 and MDA-MB-361, defying their secretion of cytokines such as FGF/FGF2, CSF3, CXCL10 and LIF. This could be explained by a strong induction of the EMT, known to gradually reduce cell proliferation [80]. In line with this notion, the mesenchymal MDA-MB-231 cells [27] showed an increased proliferation upon co-culture with ln-aT bASCs compared to ob-aT bASCs. Moreover, obese bASCs have an increased secretion of IL6, which has been shown to trigger cancer cell proliferation by activating the JAK/STAT3, ERK1/2 and STAT3/NFκB pathways in multiple cancer entities including breast cancer [81]. Finally, it was shown that myCAFs were located in a direct proximity to pancreatic tumors, whereas iCAFs were found far from neoplastic cells [82]. This suggests that ob-aT bASCs may crosstalk to breast cancer cells directly via cell-cell contact or ECM remodeling, whereas ln-aT bASCs communicate to breast cancer cells indirectly via secreted cytokines/chemokines. This assumption is further strengthened by a report showing that the direct co-culture of myCAFs increased the proliferation of various pancreatic epithelial cancer cell lines [83]. Thus, ob-aT bASCs are more capable of promoting proliferation in epithelial breast cancer cells as well as activating CSC-associated genes in mesenchymal breast cancer cells. This might help to explain, at least partially, why obesity is associated with reduced survival of postmenopausal breast cancer patients, with an increased mesenchymal/mesenchymal stem cell-like origin, and progressive cancer of premenopausal breast cancer patients with a more epithelial type [84].

CAFs, independent of their subtype, have also been described to increase tumor chemoresistance in vivo and in vitro [85, 86]. Among these different CAF subtypes, iCAFs are reported to have a particular effect on chemoresistance in breast cancer patients [40, 86], probably due to their high secretion of cytokines involved in therapy resistance, such as CXCL1–3, CCL2, CSF3, CXCL10, IL1β and LIF. These cytokines have been shown to play critical roles in regulating tumor immune tolerance [87], recruitment and de-differentiation of myeloid-derived suppressor cells [86], EMT induction [88], activation of STAT3, PI3K, MAPK and Rho signaling pathways [89], and inducing cancer stemness in breast cancer cells [90]. Indeed, ln-aT bASCs were highly effective in triggering the EMT in low-malignant BT474 cells involved in the development of chemoresistance [91] through the activation of multiple known EMT-inducing pathways, including JAK/STAT3/PI3K/TGFβ [92], as shown in the transcriptome and qPCR analysis. ob-aT bASCs exhibited an increased ability to stimulate cancer stemness in highly malignant MDA-MB-231 cells by enhancing the gene expression of pluripotency and CSC associated genes such as *ALDH1H1*, *ALDH2*, c-*MYC*, CD34, LGR5, CXCR4, *SOX2* and *OCT4* [62, 93], fueling further their malignant potential. Moreover, both ln/ob-aT bASCs stimulate the gene expression of ATM, an essential component of the DNA double-strand break repair mechanism, which may explain reduced DNA foci number and decreased apoptotic response in breast cancer cells treated with DTX, since the combination of ATM and ATR inhibitors is already used to re-sensitize breast cancer cells in clinical trials [94]. Together, bASCs may exert multiple mechanisms to increase therapy resistance, in particular, their de-differentiation into CAFs triggers EMT induction, stemness generation and increased cell survival of breast cancer cells. More investigations are warranted

to study the detailed impact of ln/ob-aT bASCs on breast cancer chemoresistance and their immunomodulatory function in vitro and in vivo.

Finally, an ex vivo correlation has been established between the expression of iCAF marker LIF and myCAF marker αSMA with breast cancer tissue sections from patients with or without obesity. Specifically, the tissue sections of obese patients displayed a significantly higher αSMA level in stroma compared to the sections from lean patients. This is of specific importance, as it has been recently reported that the stromal expression of αSMA is highly associated with the resistance to trastuzumab in patients with early-stage Her2 positive breast cancer [95]. Additionally, the expression of αSMA was found to be correlated with poor prognosis in patients with ER positive breast cancer [96] and in patients with luminal breast cancer [97], likely mediated by a TMX resistance and an increased proliferation. Moreover, the expression of LIF in the stroma was significantly elevated in breast cancer tissue sections from lean patients. Interestingly, the high expression of LIF has been connected to increased tumor progression, stemness, therapy resistance and TME modulation in various cancer entities in multiple in vitro and in vivo models [98] and the immunization against LIF or LIFR suppressed the tumor formation, growth and metastasis in a mammary xenograft mouse model [99]. Our findings clearly suggest that obesity influences the TME. These insights could be of great significance in determining the fate of breast cancer development and be useful for future targeted therapies.

Conclusion

This work demonstrates the different de-differentiation processes of bASCs in the TME of breast cancers from obese and lean patients, relative to their counterparts from cancer distant adipose tissues of the same patients to exclude individual specific features. Importantly, ln/ob-aT bASCs greatly reduce their differentiation capacity. Instead, ln-aT bASCs and ob-aT bASCs alter their transcriptome as well as secretome toward an iCAF or myCAF profile, respectively. These cancer-educated bASCs are connected to increased proliferation, motility and chemoresistance of breast cancer cell spheroids. Intriguingly, ln-aT bASCs induce the EMT in epithelial-like breast cancer cells, whereas ob-aT bASCs are more potent to enrich CSC genes in mesenchymal-like breast cancer cells (Fig. 8F), contributing further to chemotherapy resistance. Additional studies are required to corroborate these findings and their in vivo significance. It is also important to explore the precise molecular mechanisms by which the TME affects the function of bASCs in an obesity-dependent manner, and how cancer-educated bASCs fuel breast cancer progression at molecular levels.

Supplementary Information

The online version contains supplementary material available at https://doi.org/10.1186/s13046-022-02592-y.

Additional file 1: Supplementary information. Supplementary Table 1. Clinical information of breast cancer patients, whose mammary adipose tissues were used for bASC isolation. **Supplementary Table 2.** Cell surface markers of different lean bASCs. **Supplementary Table 3.** Cell surface markers of different obese bASCs. **Supplementary Table 4.** Clinical information of breast cancer patients, whose mammary adipose tissues were used for IHC staining. **Figure S1.** No obvious alterations in cell cycle distribution and cell viability among various bASC subgroups, and more COLA1 and vimentin in aT-bASCs than in dT-bASCs. **Figure S2.** Both ln- and ob-aT bASCs display deregulated differentiated associated genes and ln-aT bASCs increased iCAF genes. **Figure S3.** Secretion of bASCs alone or upon incubation with MDA-MB-231 cells. **Figure S4**. ob- and ln-aT bASCs promote the growth of BT474 spheroids. **Figure S5.** Direct co-culture of ob- and ln-aT bASCs promotes the growth of BT474 and MDA-MB-361 spheroids. **Figure S6:** Ob- and ln-aT bASCs promote proliferation of MDA-MB-361 spheroids and their supernatants enhance the motility of breast cancer cells. **Figure S7.** bASCs promote the formation and growth of spheroids of breast cancer cells. **Figure S8.** Hybrid spheroids of breast cancer cells and bASCs demonstrate an increased resistance to chemotherapeutic agents. **Figure S9.** Transcriptome profiles of triple negative MDA-MB-231 cells directly co-cultured with bASCs. **Figure S10.** ln-aT bASCs efficiently trigger EMT in epithelial breast cancer cell lines, while ob-aT bASCs more efficiently stimulate MDA-MB-231 cells into a CSC phenotype.

Acknowledgements

We are grateful to our patients and our clinical team for making this study possible.

Authors' contributions

JY, AR, and CS conceived and supervised the project. AR designed the experiments. AR, SR, AF, NNK, and BKS performed the experiments. AR and SR analyzed the data. SCH, JW, RA, FL and CS collected samples and clinical information. AR wrote the initial manuscript. JY and NNK modified the manuscript. JY and NNK did critical reading. All authors read and approved the final manuscript.

Funding

Open Access funding enabled and organized by Projekt DEAL. This project was funded by the "Deutsche Forschungsgemeinschaft "(DFG, German Research Foundation, project number 413992926).

Availability of data and materials

All data generated or analyzed during this study are included in this article and its supplementary information.

Declarations

Ethics approval and consent to participate

The collection of breast adipose tissues and breast tumor tissue was approved by the Ethics Committee of the Johann Wolfgang Goethe University Hospital Frankfurt (reference numbers: 443/11 and 4/09). Informed written consents were obtained from all donors.

Consent for publication

Not applicable.

Competing interests

The authors declare that they have no competing interests.

Author details

[1]Obstetrics and Prenatal Medicine, Gynecology and Obstetrics, University Hospital Frankfurt, J. W. Goethe-University, Theodor-Stern-Kai 7, D-60590 Frankfurt, Germany.

Received: 26 September 2022 Accepted: 29 December 2022
Published online: 30 January 2023

References

1. Malik VS, Willet WC, Hu FB. Nearly a decade on - trends, risk factors and policy implications in global obesity. Nat Rev Endocrinol. 2020;16(11):615–6.
2. Bixby H, Bentham J, Zhou B, Di Cesare M, Paciorek CJ, Bennett JE, et al. Rising rural body-mass index is the main driver of the global obesity epidemic in adults. Nature. 2019;569(7755):260.
3. Wang LM, Zhou B, Zhao ZP, Yang L, Zhang M, Jiang Y, et al. Body-mass index and obesity in urban and rural China: findings from consecutive nationally representative surveys during 2004-18. Lancet. 2021;398(10294):53–63.
4. Garcia-Estevez L, Cortes J, Perez S, Calvo I, Gallegos I, Moreno-Bueno G. Obesity and breast Cancer: a paradoxical and controversial relationship influenced by menopausal status. Front Oncol. 2021;11:705911.
5. Kim M, Lee C, Park J. Extracellular matrix remodeling facilitates obesity-associated cancer progression. Trends Cell Biol. 2022;32(10):825–34.
6. Huang S, Rutkowsky JM, Snodgrass RG, Ono-Moore KD, Schneider DA, Newman JW, et al. Saturated fatty acids activate TLR-mediated proinflammatory signaling pathways. J Lipid Res. 2012;53(9):2002–13.
7. Howe LR, Subbaramaiah K, Hudis CA, Dannenberg AJ. Molecular pathways: adipose inflammation as a mediator of obesity-associated cancer. Clin Cancer Res. 2013;19(22):6074–83.
8. Xu L, Kitade H, Ni Y, Ota T. Roles of chemokines and chemokine receptors in obesity-associated insulin resistance and nonalcoholic fatty liver disease. Biomolecules. 2015;5(3):1563–79.
9. Louwen F, Ritter A, Kreis NN, Yuan J. Insight into the development of obesity: functional alterations of adipose-derived mesenchymal stem cells. Obes Rev. 2018;19(7):888–904.
10. Hillers-Ziemer LE, Kuziel G, Williams AE, Moore BN, Arendt LM. Breast cancer microenvironment and obesity: challenges for therapy. Cancer Metastasis Rev. 2022;41(3):627–47.
11. Zhao H, Wang J, Fang D, Lee O, Chatterton RT, Stearns V, et al. Adiposity results in metabolic and inflammation differences in premenopausal and postmenopausal women consistent with the difference in breast Cancer risk. Horm Cancer. 2018;9(4):229–39.
12. Ringel AE, Drijvers JM, Baker GJ, Catozzi A, García-Cañaveras JC, Gassaway BM, et al. Obesity shapes metabolism in the tumor microenvironment to suppress anti-tumor immunity. Cell. 2020;183(7):1848–1866.e1826.
13. Danenberg E, Bardwell H, Zanotelli VRT, Provenzano E, Chin S-F, Rueda OM, et al. Breast tumor microenvironment structures are associated with genomic features and clinical outcome. Nat Genet. 2022;54(5):660–9.
14. Lin HJ, Liu YG, Lofland D, Lin JY. Breast Cancer tumor microenvironment and molecular aberrations hijack Tumoricidal immunity. Cancers. 2022;14(2):285.
15. Salemme V, Centonze G, Cavallo F, Defilippi P, Conti L. The crosstalk between tumor cells and the immune microenvironment in breast Cancer: implications for immunotherapy. Front Oncol. 2021;11:610303.
16. Sahai E, Astsaturov I, Cukierman E, DeNardo DG, Egeblad M, Evans RM, et al. A framework for advancing our understanding of cancer-associated fibroblasts. Nat Rev Cancer. 2020;20(3):174–86.
17. Elwakeel E, Weigert A. Breast Cancer CAFs: spectrum of phenotypes and promising targeting avenues. Int J Mol Sci. 2021;22(21):11636.
18. Galland S, Stamenkovic I. Mesenchymal stromal cells in cancer: a review of their immunomodulatory functions and dual effects on tumor progression. J Pathol. 2020;250(5):555–72.
19. Ugurlu B, Karaoz E. Comparison of similar cells: mesenchymal stromal cells and fibroblasts. Acta Histochem. 2020;122(8):151634.
20. Ritter A, Friemel A, Fornoff F, Adjan M, Solbach C, Yuan J, et al. Characterization of adipose-derived stem cells from subcutaneous and visceral adipose tissues and their function in breast cancer cells. Oncotarget. 2015;6(33):34475–93.
21. Najar M, Fayyad-Kazan H, Faour WH, Badran B, Journe F, Lagneaux L. Breast cancer cells and bone marrow mesenchymal stromal cells: a regulated modulation of the breast tumor in the context of immune response. Inflamm Res. 2017;66(2):129–39.
22. Lee H-Y, Hong I-S. Double-edged sword of mesenchymal stem cells: Cancer-promoting versus therapeutic potential. Cancer Sci. 2017;108(10):1939–46.
23. Cho K-A, Park M, Kim Y-H, Woo S-Y, Ryu K-H. RNA sequencing reveals a transcriptomic portrait of human mesenchymal stem cells from bone marrow, adipose tissue, and palatine tonsils. Sci Rep. 2017;7(1):17114.
24. Ritter A, Friemel A, Roth S, Kreis NN, Hoock SC, Safdar BK, et al. Subcutaneous and visceral adipose-derived mesenchymal stem cells: commonality and diversity. Cells. 2019;8(10):1288.
25. Hass R. Role of MSC in the tumor microenvironment. Cancers. 2020;12(8):2107.
26. Mueller MM, Fusenig NE. Friends or foes - bipolar effects of the tumour stroma in cancer. Nat Rev Cancer. 2004;4(11):839–49.
27. Dai X, Cheng H, Bai Z, Li J. Breast Cancer cell line classification and its relevance with breast tumor subtyping. J Cancer. 2017;8(16):3131–41.
28. Ritter A, Roth S, Kreis NN, Friemel A, Hoock SC, Souto AS, et al. Primary cilia in trophoblastic cells potential involvement in preeclampsia. Hypertension. 2020;76(5):1491–505.
29. Ritter A, Friemel A, Kreis NN, Louwen F, Yuan J. Impact of polo-like kinase 1 inhibitors on human adipose tissue-derived mesenchymal stem cells. Oncotarget. 2016;7(51):84271–85.
30. Klimczak A, Kozlowska U. Mesenchymal stromal cells and tissue-specific progenitor cells: their role in tissue homeostasis. Stem Cells Int. 2016;2016:4285215.
31. Vizoso FJ, Eiro N, Costa L, Esparza P, Landin M, Diaz-Rodriguez P, et al. Mesenchymal stem cells in homeostasis and systemic diseases: hypothesis, evidences, and therapeutic opportunities. Int J Mol Sci. 2019;20(15):3738.
32. Ritter A, Friemel A, Kreis NN, Hoock SC, Roth S, Kielland-Kaisen U, et al. Primary cilia are dysfunctional in obese adipose-derived mesenchymal stem cells. Stem Cell Rep. 2018;10(2):583–99.
33. Ritter A, Kreis N-N, Roth S, Friemel A, Jennewein L, Eichbaum C, et al. Restoration of primary cilia in obese adipose-derived mesenchymal stem cells by inhibiting Aurora a or extracellular signal-regulated kinase. Stem Cell Res Ther. 2019;10(1):255–5.
34. Cizkova K, Foltynkova T, Gachechiladze M, Tauber Z. Comparative analysis of Immunohistochemical staining intensity determined by light microscopy, ImageJ and QuPath in placental Hofbauer cells. Acta Histochem Cytochem. 2021;54(1):21–9.
35. Dominici M, Le Blanc K, Mueller I, Slaper-Cortenbach I, Marini F, Krause D, et al. Minimal criteria for defining multipotent mesenchymal stromal cells. The international society for cellular therapy position statement. Cytotherapy. 2006;8(4):315–7.
36. Jin MZ, Jin WL. The updated landscape of tumor microenvironment and drug repurposing. Signal Transduct Target Ther. 2020;5(1):166.
37. Hill BS, Pelagalli A, Passaro N, Zannetti A. Tumor-educated mesenchymal stem cells promote pro-metastatic phenotype. Oncotarget. 2017;8(42):73296–311.
38. Ping Q, Yan R, Cheng X, Wang W, Zhong Y, Hou Z, et al. Cancer-associated fibroblasts: overview, progress, challenges, and directions. Cancer Gene Ther. 2021;28(9):984–99.
39. Orimo A, Gupta PB, Sgroi DC, Arenzana-Seisdedos F, Delaunay T, Naeem R, et al. Stromal fibroblasts present in invasive human breast carcinomas promote tumor growth and angiogenesis through elevated SDF-1/CXCL12 secretion. Cell. 2005;121(3):335–48.
40. Kieffer Y, Hocine HR, Gentric G, Pelon F, Bernard C, Bourachot B, et al. Single-cell analysis reveals fibroblast clusters linked to immunotherapy resistance in Cancer. Cancer Discov. 2020;10(9):1330–51.
41. Sebastian A, Hum NR, Martin KA, Gilmore SF, Peran I, Byers SW, et al. Single-cell transcriptomic analysis of tumor-derived fibroblasts and Normal tissue-resident fibroblasts reveals fibroblast heterogeneity in breast Cancer. Cancers. 2020;12(5):1307.
42. Grauel AL, Nguyen B, Ruddy D, Laszewski T, Schwartz S, Chang J, et al. TGF beta-blockade uncovers stromal plasticity in tumors by revealing the existence of a subset of interferon-licensed fibroblasts. Nat Commun. 2020;11(1):6315.
43. Ritter A, Safdar BK, Jasmer B, Kreis NN, Friemel A, Roth S, et al. The function of oncogene B-cell lymphoma 6 in the regulation of the migration and invasion of trophoblastic cells. Int J Mol Sci. 2020;21(21):8393.
44. Wang N, Liu W, Zheng Y, Wang S, Yang B, Li M, et al. CXCL1 derived from tumor-associated macrophages promotes breast cancer metastasis via activating NF-κB/SOX4 signaling. Cell Death Dis. 2018;9(9):880.

45. Romero-Moreno R, Curtis KJ, Coughlin TR, Miranda-Vergara MC, Dutta S, Natarajan A, et al. The CXCL5/CXCR2 axis is sufficient to promote breast cancer colonization during bone metastasis. Nat Commun. 2019;10(1):4404.
46. Nurmik M, Ullmann P, Rodriguez F, Haan S, Letellier E. In search of definitions: Cancer-associated fibroblasts and their markers. Int J Cancer. 2020;146(4):895–905.
47. Monteran L, Erez N. The dark side of fibroblasts: Cancer-associated fibroblasts as mediators of immunosuppression in the tumor microenvironment. Front Immunol. 2019;10:1835.
48. Hillers LE, D'Amato JV, Chamberlin T, Paderta G, Arendt LM. Obesity-activated adipose-derived stromal cells promote breast Cancer growth and invasion. Neoplasia. 2018;20(11):1161–74.
49. Morein D, Erlichman N, Ben-Baruch A. Beyond cell motility: the expanding roles of chemokines and their receptors in malignancy. Front Immunol. 2020;11:952.
50. Wu J, Ivanov AI, Fisher PB, Fu Z. Polo-like kinase 1 induces epithelial-to-mesenchymal transition and promotes epithelial cell motility by activating CRAF/ERK signaling. Elife. 2016;5:e10734.
51. Cooper AJ, Sequist LV, Lin JJ. Third-generation EGFR and ALK inhibitors: mechanisms of resistance and management. Nat Rev Clin Oncol. 2022;19(8):499–514.
52. Hagenaars SC, Vangangelt KMH, Van Pelt GW, Karancsi Z, Tollenaar RAEM, Green AR, et al. Standardization of the tumor-stroma ratio scoring method for breast cancer research. Breast Cancer Res Tr. 2022;193(3):545–53.
53. Liang W, Chen X, Zhang S, Fang J, Chen M, Xu Y, et al. Mesenchymal stem cells as a double-edged sword in tumor growth: focusing on MSC-derived cytokines. Cell Mol Biol Lett. 2021;26(1):3.
54. Harbeck N, Penault-Llorca F, Cortes J, Gnant M, Houssami N, Poortmans P, et al. Breast Cancer. Nat Rev Dis Primers. 2019;5(1):66.
55. Stope MB. Phosphorylation of histone H2A.X as a DNA-associated biomarker (review). World Acad Sci J. 2021;3(3):31.
56. Villegas VE, Rondon-Lagos M, Annaratone L, Castellano I, Grismaldo A, Sapino A, et al. Tamoxifen treatment of breast Cancer cells: impact on hedgehog/GLI1 signaling. Int J Mol Sci. 2016;17(3):308.
57. Ritter A, Kreis NN, Hoock SC, Solbach C, Louwen F, Yuan J. Adipose Tissue-Derived Mesenchymal Stromal/Stem Cells, Obesity and the Tumor Microenvironment of Breast Cancer. Cancers (Basel). 2022;14(16):3908. https://doi.org/10.3390/cancers14163908.
58. Campaner S, Amati B. Two sides of the Myc-induced DNA damage response: from tumor suppression to tumor maintenance. Cell Div. 2012;7(1):6.
59. Matthews HK, Bertoli C, de Bruin RAM. Cell cycle control in cancer. Nat Rev Mol Cell Biol. 2022;23(1):74–88.
60. Zhou HM, Zhang JG, Zhang X, Li Q. Targeting cancer stem cells for reversing therapy resistance: mechanism, signaling, and prospective agents. Signal Transduct Target Ther. 2021;6(1):62.
61. De Las RJ, Brozovic A, Izraely S, Casas-Pais A, Witz IP, Figueroa A. Cancer drug resistance induced by EMT: novel therapeutic strategies. Arch Toxicol. 2021;95(7):2279–97.
62. Zheng Q, Zhang M, Zhou F, Zhang L, Meng X. The breast Cancer stem cells traits and drug resistance. Front Pharmacol. 2020;11:599965.
63. Rizzardi AE, Johnson AT, Vogel RI, Pambuccian SE, Henriksen J, Skubitz APN, et al. Quantitative comparison of immunohistochemical staining measured by digital image analysis versus pathologist visual scoring. Diagn Pathol. 2012;7(1):42.
64. Li W, Ren G, Huang Y, Su J, Han Y, Li J, et al. Mesenchymal stem cells: a double-edged sword in regulating immune responses. Cell Death Differ. 2012;19(9):1505–13.
65. Rowan BG, Gimble JM, Sheng M, Anbalagan M, Jones RK, Frazier TP, et al. Human adipose tissue-derived stromal/stem cells promote migration and early metastasis of triple negative breast cancer xenografts. PLoS One. 2014;9(2):e89595.
66. Goto H, Shimono Y, Funakoshi Y, Imamura Y, Toyoda M, Kiyota N, et al. Adipose-derived stem cells enhance human breast cancer growth and cancer stem cell-like properties through adipsin. Oncogene. 2019;38(6):767–79.
67. Le Naour A, Prat M, Thibault B, Mevel R, Lemaitre L, Leray H, et al. Tumor cells educate mesenchymal stromal cells to release chemoprotective and immunomodulatory factors. J Mol Cell Biol. 2020;12(3):202–15.
68. Sai B, Dai Y, Fan S, Wang F, Wang L, Li Z, et al. Cancer-educated mesenchymal stem cells promote the survival of cancer cells at primary and distant metastatic sites via the expansion of bone marrow-derived-PMN-MDSCs. Cell Death Dis. 2019;10(12):941.
69. Rey F, Lesma E, Massihnia D, Ciusani E, Nava S, Vasco C, et al. Adipose-derived stem cells from fat tissue of breast Cancer microenvironment present altered Adipogenic differentiation capabilities. Stem Cells Int. 2019;2019:1480314.
70. Liang X, Ding Y, Lin F, Zhang Y, Zhou X, Meng Q, et al. Overexpression of ERBB4 rejuvenates aged mesenchymal stem cells and enhances angiogenesis via PI3K/AKT and MAPK/ERK pathways. FASEB J. 2019;33(3):4559–70.
71. Sun H, Dai K, Tang T, Zhang X. Regulation of osteoblast differentiation by slit2 in osteoblastic cells. Cells Tissues Organs. 2009;190(2):69–80.
72. Julian LM, Blais A. Transcriptional control of stem cell fate by E2Fs and pocket proteins. Front Genet. 2015;6:161–1.
73. Popov B, Petrov N. pRb-E2F signaling in life of mesenchymal stem cells: cell cycle, cell fate, and cell differentiation. Genes Dis. 2014;1(2):174–87.
74. Conley SM, Hickson LJ, Kellogg TA, McKenzie T, Heimbach JK, Taner T, et al. Human obesity induces dysfunction and early senescence in adipose tissue-derived mesenchymal stromal/stem cells. Front Cell Dev Biol. 2020;8:197.
75. Bhattacharjee S, Hamberger F, Ravichandra A, Miller M, Nair A, Affo S, et al. Tumor restriction by type I collagen opposes tumor-promoting effects of cancer-associated fibroblasts. J Clin Invest. 2021;131(11):e146987. https://doi.org/10.1172/JCI146987.
76. Zeltz C, Alam J, Liu H, Erusappan PM, Hoschuetzky H, Molven A, et al. α11β1 integrin is induced in a subset of Cancer-associated fibroblasts in desmoplastic tumor stroma and mediates in vitro cell migration. Cancers. 2019;11(6):765.
77. Biffi G, Tuveson DA. Diversity and biology of Cancer-associated fibroblasts. Physiol Rev. 2021;101(1):147–76.
78. Strong AL, Pei DT, Hurst CG, Gimble JM, Burow ME, Bunnell BA. Obesity enhances the conversion of adipose-derived stromal/stem cells into carcinoma-associated fibroblast leading to Cancer cell proliferation and progression to an invasive phenotype. Stem Cells Int. 2017;2017:9216502.
79. Hartupee J, Mann DL. Role of inflammatory cells in fibroblast activation. J Mol Cell Cardiol. 2016;93:143–8.
80. Pastushenko I, Blanpain C. EMT transition states during tumor progression and metastasis. Trends Cell Biol. 2019;29(3):212–26.
81. Wu F, Yang J, Liu J, Wang Y, Mu J, Zeng Q, et al. Signaling pathways in cancer-associated fibroblasts and targeted therapy for cancer. Signal Transduct Target Ther. 2021;6(1):218.
82. Öhlund D, Handly-Santana A, Biffi G, Elyada E, Almeida AS, Ponz-Sarvise M, et al. Distinct populations of inflammatory fibroblasts and myofibroblasts in pancreatic cancer. J Exp Med. 2017;214(3):579–96.
83. Begum A, McMillan RH, Chang YT, Penchev VR, Rajeshkumar NV, Maitra A, et al. Direct interactions with Cancer-associated fibroblasts Lead to enhanced pancreatic Cancer stem cell function. Pancreas. 2019;48(3):329–34.
84. Bareche Y, Venet D, Ignatiadis M, Aftimos P, Piccart M, Rothe F, et al. Unravelling triple-negative breast cancer molecular heterogeneity using an integrative multiomic analysis. Ann Oncol. 2018;29(4):895–902.
85. Jena BC, Das CK, Bharadwaj D, Mandal M. Cancer associated fibroblast mediated chemoresistance: a paradigm shift in understanding the mechanism of tumor progression. Biochim Biophys Acta Rev Cancer. 2020;1874(2):188416.
86. Mao X, Xu J, Wang W, Liang C, Hua J, Liu J, et al. Crosstalk between cancer-associated fibroblasts and immune cells in the tumor microenvironment: new findings and future perspectives. Mol Cancer. 2021;20(1):131.
87. Jiang H, Hegde S, DeNardo DG. Tumor-associated fibrosis as a regulator of tumor immunity and response to immunotherapy. Cancer Immunol Immunother. 2017;66(8):1037–48.
88. Rogic A, Pant I, Grumolato L, Fernandez-Rodriguez R, Edwards A, Das S, et al. High endogenous CCL2 expression promotes the aggressive phenotype of human inflammatory breast cancer. Nat Commun. 2021;12(1):6889.
89. Chen W, Qin Y, Liu S. Cytokines, breast cancer stem cells (BCSCs) and chemoresistance. Clin Transl Med. 2018;7(1):27.
90. Loh JJ, Ma S. The role of Cancer-associated fibroblast as a dynamic player in mediating Cancer Stemness in the tumor microenvironment. Front Cell Dev Biol. 2021;9:727640.
91. Dudas J, Ladanyi A, Ingruber J, Steinbichler TB, Riechelmann H. Epithelial to mesenchymal transition: a mechanism that fuels Cancer radio/Chemoresistance. Cells. 2020;9(2):428.

92. Dongre A, Weinberg RA. New insights into the mechanisms of epithelial–mesenchymal transition and implications for cancer. Nat Rev Mol Cell Biol. 2019;20(2):69–84.
93. Song K, Farzaneh M. Signaling pathways governing breast cancer stem cells behavior. Stem Cell Res Ther. 2021;12(1):245.
94. Li LY, Guan YD, Chen XS, Yang JM, Cheng Y. DNA repair pathways in Cancer therapy and resistance. Front Pharmacol. 2020;11:629266.
95. Vathiotis IA, Moutafi MK, Divakar P, Aung TN, Qing T, Fernandez A, et al. Alpha-smooth muscle actin expression in the stroma predicts resistance to Trastuzumab in patients with early-stage HER2-positive breast Cancer. Clin Cancer Res. 2021;27(22):6156–63.
96. Kim S, You D, Jeong Y, Yu J, Kim SW, Nam SJ, et al. TP53 upregulates α-smooth muscle actin expression in tamoxifen-resistant breast cancer cells. Oncol Rep. 2019;41(2):1075–82.
97. Muchlińska A, Nagel A, Popęda M, Szade J, Niemira M, Zieliński J, et al. Alpha-smooth muscle actin-positive cancer-associated fibroblasts secreting osteopontin promote growth of luminal breast cancer. Cell Mol Biol Lett. 2022;27(1):45.
98. Viswanadhapalli S, Dileep KV, Zhang KYJ, Nair HB, Vadlamudi RK. Targeting LIF/LIFR signaling in cancer. Genes Dis. 2022;9(4):973–80.
99. Ghanei Z, Mehri N, Jamshidizad A, Joupari MD, Shamsara M. Immunization against leukemia inhibitory factor and its receptor suppresses tumor formation of breast cancer initiating cells in BALB/c mouse. Sci Rep. 2020;10(1):11465.

Publisher's Note